

QCD, Gravitational Waves, and Pulsars

Partha Bagchi*

School of Physical Sciences, National Institute of Science Education and Research, Jatni, Odisha -752050, India

Oindrila Ganguly†

The Institute of Mathematical Sciences, Chennai -600113, India

Biswanath Layek‡

Department of Physics, Birla Institute of Technology and Science, Pilani -333031, India

Anjishnu Sarkar§

Physics Department, The LNM Institute of Information Technology, Jaipur -302031, India

Ajit M. Srivastava¶

Institute of Physics, Bhubaneswar-751005, India

Investigations of the phase diagram of quantum chromodynamics (QCD) have revealed exotic new possibilities. Experimental investigations with relativistic heavy ion collision experiments (RHICE) have been able to probe relatively low baryon chemical potential regime of the QCD phase diagram, namely the quark-gluon plasma (QGP) phase. An entire new spectrum of phases is expected to arise at very high baryon chemical potential, which may remain out of reach at these terrestrial experiments. These phases are collectively referred to as *color superconducting phases*. Attention is naturally directed towards astrophysics where gravity assisted ultra high baryon density objects naturally occur. The densest such object, which can be directly observed, is a neutron star. It is thus speculated that cores of neutron stars provide a natural laboratory where such exotic phases of QCD may exist. In fact, the theoretically well established *neutron superfluidity phase* is also believed to be found only inside neutron stars. Focus on neutrons stars has tremendously intensified in recent years from a completely different angle. Even though the first *indirect* detection of gravitational waves had come long ago from a binary neutron star (BNS) system, it is the direct detection of gravitational waves by LIGO/Virgo from BNS merger events which has allowed the possibility of directly probing the properties of the interior of a neutron star. A truly remarkable phenomenon manifested by rapidly rotating neutron stars is in their *avatar* as *Pulsars*. The accuracy of pulsar timing can reach the level of one part in 10^{15} , comparable to that of atomic clocks. Indeed, it was such a great accuracy which had allowed the first indirect detection of gravitational waves from a BNS system. Such an incredible accuracy of pulse timings points to a very interesting possibility. Any deformation of the pulsar, even if it is extremely tiny, has the potential of leaving its imprints on the pulses through introduction of tiny perturbations in the entire moment of inertial (MI) tensor. While, the diagonal components of perturbed MI tensor affect the pulse timings, the off-diagonal components lead to wobbling of pulsar, directly affecting the pulse profile. This opens up a new window of opportunity for exploring various phase transitions occurring inside a pulsar core, through induced density fluctuations, which may be observable as perturbations in the pulse timing as well as its profile. Such perturbations also naturally induce a rapidly changing quadrupole moment of the star, thereby providing a new source of gravitational wave emission. Another remarkable possibility arises when we consider the effect of an external gravitational wave on neutron star. With the possibility of detecting any minute changes in its configuration through pulse observations, the neutron star has the potential of performing as a Weber detector of gravitational wave. This brief review will focus on these specific aspects of a pulsar. Specifically, the focus will be on the type of physics which can be probed by utilizing the effect of changes in the MI tensor of the pulsar on pulse properties.

PACS numbers: 12.38.Mh,97.60.Gb,95.55.Ym,04.80.Nn,26.60.+c

I. INTRODUCTION

Cosmos has always proved to be the ultimate laboratory where physical systems may exist in extreme environments, even those which are beyond the reach of any terrestrial experiments. Early hot and dense stages of the Universe is one such case where extremely high temperatures are achieved. Fortunately, some of those

* parphy85@gmail.com

† oindrila@gmail.com

‡ layek@pilani.bits-pilani.ac.in

§ anjishnu@lnmiit.ac.in

¶ ajit@iopb.res.in

stages, with temperatures reaching 10^{12} K (few hundred MeV) are possible to be partially probed in terrestrial experiments now in relativistic heavy-ion collision experiments (RHICE) [1, 2]. This possibility has put the physics of quark-gluon plasma (QGP) phase of QCD matter at a central stage, the phase which is believed to exist in the Universe when it was few tens of microseconds old. Experimental observations at RHICE have already shown completely unexpected results, for example, a near-perfect fluid nature of QGP with a value of shear viscosity to entropy ratio which is close to the proposed lowest bound on this number [3]. With continued efforts in RHICE with varying collision energy, it has been possible to extensively investigate certain part of the phase diagram of quantum chromodynamics (QCD) which corresponds to relatively low baryon number density. As the early Universe was filled with a matter with extremely low baryon number density, it allows one to claim that conditions like early Universe have been recreated in laboratory (at least for the strongly interacting matter part).

At the same time, theoretical investigations have revealed the possibility of an entire new spectrum of phases of strongly interacting matter which are expected to arise at very high baryon chemical potential [4]. It is reasonably clear now that much of this extremely rich part of the QCD phase diagram may remain out of reach at these terrestrial experiments. These phases are collectively referred to as the *color superconducting phases* [5, 6]. Attention is thus naturally directed towards astrophysics where gravity assisted ultra high baryon density objects routinely occur. Extreme conditions of high baryon density are expected to be reached in supernova explosions, in neutrons stars, and in matter undergoing collapse to a black hole. The densest such object, which can be directly observed at present, is a neutron star. It is speculated that cores of neutron stars provide a natural laboratory where various exotic phases of QCD may occur [7]. Even exotic forms of matter, stable only under extreme conditions of density and pressure, may form in these objects, such as strange stars [8–12]. Interestingly, the theoretically very well established *neutron superfluidity phase* has never been seen in any terrestrial experiment. At the same time it is expected to routinely occur inside neutron stars [13]. In fact, superfluid vortices in such a phase provide the most convincing explanation of the phenomena of pulsar glitches [14].

Neutron stars have long been investigated theoretically and experimentally, especially with pulsar observations. Pulsars are rapidly rotating neutron stars with pulse timings which are observed on earth with incredible accuracy, reaching one part in 10^{15} for certain pulsars, comparable to that of atomic clocks. This extreme accuracy of pulse timings had allowed the first indirect detection of gravitational waves from a binary neutron star (BNS) system [15, 16]. Neutron star physics has acquired a centre stage recently with the advent of gravitational wave detectors. After the first direct detection of gravitational waves (GWs) by LIGO coming from a binary black hole

merger event [17], the stage was set for the detection of GWs from spiral-in of other compact dense objects. The first such event of binary neutron star merger was detected by LIGO/Virgo in 2017 [18] and that opened the remarkable possibility of directly probing the properties of the interior of neutron stars.

Neutron stars thus acquire a unique status of providing a laboratory for probing microphysics of exotic phases of QCD on one hand, while providing a window to probe the physics of its interior using GW detectors on earth in BNS merger events on the other. This remarkable story of neutron stars still allows for one more chapter, that relating to its *avatar* as a pulsar with extreme accuracy of pulsar timing observations. Such an incredible accuracy of pulse timings points to a very interesting possibility. Any deformation of the neutron star, even if it is extremely tiny, has the potential of leaving its imprints on the pulses through introduction of tiny perturbations in the entire moment of inertial (MI) tensor. Clearly, it will directly affect the pulse timing. However, a general deformation of NS will change the entire MI tensor, including its off-diagonal components. The diagonal components of perturbed MI tensor will affect the pulse timings, at the same time, the perturbed off-diagonal components will induce wobbling of pulsar. Wobbling of pulsar (on top of any previously present) will directly affect the profile of pulses as observed on earth. Thus observations of changes in pulse timings, along with any accompanying changes in the pulse profile will contain information about details of minute changes in the configuration of NS, e.g. density perturbations inside the NS, or its overall deformations. This opens up a new window of opportunity for exploring various phase transitions occurring inside a pulsar core, through induced density fluctuations, which may be observable as perturbations in the pulse timing as well as its profile [19–21]. Such perturbations also naturally induce a rapidly changing quadrupole moment of the star, thereby providing a new source of gravitational wave emission [19]. Another remarkable possibility arises when we consider the effect of an external gravitational wave on neutron star. With the possibility of detecting any minute changes in its configuration through pulse observations, the neutron star has the potential of performing as a Weber detector of gravitational wave [22]. The possibility of such *Weber* detectors, spread out in space, with their signals (carrying imprints of any GWs) monitored at earth, has tremendous potential, especially in allowing us to re-visit GW events whose signal may have passed through earth in past [23].

In this brief review we will focus on this particular aspect of NS physics, namely the range of phenomena which can be probed utilizing the effect of changes in the configuration of NS using high precision measurements of pulses coming from a pulsar. We will begin in Section II with a discussion of salient features of the QCD phase diagram, specially the high baryon density regime. We will briefly discuss theoretical expectations of different phases

in this regime. We will also connect with the experimental situation and discuss what parts of QCD phase diagram can be probed by the present and future relativistic heavy-ion collision experiments, and which regimes may remain out of reach of these terrestrial experiments, leading us towards cosmos, in particular to neutron stars. Section III will then be devoted to basic physics of neutron stars, including the superfluid phase in its interior as well as the possibility of exotic QCD phases in the inner core. There are excellent reviews on this subject (as well as on the subject matter of Section II, i.e. QCD phase diagram). We will only recollect essential parts of these discussions for self-completeness of the discussion here. Thus, we will also briefly discuss how recent gravitational wave detections have allowed the probe of NS interior properties. Section IV will be devoted to pulsars recalling the extreme accuracy of pulsar timing observations. We will also recall here the first (indirect) detection of gravitational waves (GWs) by pulsar observations, as well as ongoing attempts of pulsar timing arrays for detection of ultra low frequency GWs. In Section V we will discuss various proposals from the literature for possible observational signatures of various phases in NS interiors. Among these, glitches take a prominent role as well established signals for the existence of superfluid phase in NS interior. We will discuss here difficulty of this explanation in accounting for relatively recent observations of anti-glitches. We will also discuss various proposals for detection of the exotic color superconducting phases of QCD in NS interior. Here we will also point to a new possibility where possibly the highest observable baryon density phases could arise, that is in the matter undergoing collapse to a black hole. For example, for a stellar mass black hole, the Schwarzschild radius is about one third of the typical neutron star radius. Thus it is possible that baryon densities in matter collapsing to black hole may become about 20 times larger than that in a neutron star (depending on the density profile, also the density contrast will be smaller for a more massive black hole). Certainly, it will only be transient, lasting only for tiny fractions of seconds, but still may allow observational signatures of novel QCD phase transition which can occur with typical local time scale of QCD, i.e. fm/c.

In Section VI we will discuss the implications of phase transitions occurring inside a pulsar on its pulses. The consequences of phase transition (for example from nuclear matter to QGP) occurring in the core of a neutron star in terms of its effect on the moment of inertia have been discussed in the literature with its observational implications on the spin rate of the neutron star [24, 25]. These discussions primarily focused on the change in the equation of state during the phase transition, and hence the main implications related to changes in the diagonal components of the moment of inertia tensor affecting the spin rate of the neutron star. However, phase transitions necessarily produce density fluctuations, which perturb entire moment of inertia tensor, including its off-diagonal components. This was discussed by some of us in [19, 20],

pointing out that phase transitions induced density fluctuations modify the entire moment of inertia tensor of the pulsar which affects pulse timings, but also induces modulations of the pulse profile. The detailed modification of the pulses carries the information of statistical nature of density fluctuations, and hence the precise nature of phase transition occurring inside the NS interior. In Section VII we will discuss a special case in detail when the density fluctuations are modelled in terms of random components of MI tensor added to the unperturbed diagonal MI tensor of the neutron star [21]. We will see here the effect on pulse timings as well as the nature of modulations expected in the pulse profile. We will discuss that even for very tiny density fluctuations, even if pulsar timings remain extremely small, pulse profile modification may become relatively large. This is because while pulse timing changes will be proportional to typical density fluctuation magnitude ϵ , the pulse profile modification will be proportional to ϵ/η^2 where η is the NS deformation parameter. (η is typically very small $\sim 10^{-8} - 10^{-4}$. This observation will play an important role in later discussion when we discuss possible detection of external GWs using NS deformations.) We will also briefly discuss how the same technique can be used to detect other perturbations occurring in neutron stars, e.g. collision with an asteroid.

In Section VIII we will discuss how phase transitions occurring inside NS may provide a new *high frequency* source of GWs through density fluctuation induced rapidly changing quadrupole moment. Section IX will change the direction of discussion towards the effects of an external gravitational wave on the neutron star configuration. Clearly, expected deformations in NS will be extremely tiny. However, we will discuss how it may be possible to detect even such tiny deformations utilizing the impressive accuracy of pulsar timing observations, and in particular possible changes in the pulse profile from induced wobbling of pulsar (recalling discussion from the results of Section VII that even if pulse timing changes remain very small, pulse profile modulations may become relatively large). We will therefore conclude in this section that pulsars will effectively act as *remotely stationed* Weber detectors whose GW perturbed signals may be observable on earth [22]. A very important part of discussion here will involve the so called *ringing* of the pulsar which will allow folding of very large number of pulses, thereby tremendously increasing the signal to noise ratio, exactly what is done in a Weber detector. We will make a point here on the importance of the quantity the *Quality factor Q* of the NS matter which will directly determine the strength of the ringing effect. While much focus has been there in the literature in calculating the shear viscosity to entropy ratio of the QCD matter (in the QGP phase as well as the hadronic phase), there is no such discussion for the Quality factor **Q**.

This possibility of pulsars acting as Weber detectors, spread in cosmos will lead to a truly remarkable possibility of re-visiting past GW events. We will discuss this

in Section X, how some GW event (collisions of black holes, neutron stars, supernova explosions etc.) from far away, whose signal may have passed through earth in past, may become observable on earth again via observations of certain pulsars which also get affected by the same GW source, and transmit the perturbed pulses which are then later detected on earth [23]. Knowing the location of GW source and various pulsar coordinates, it is possible to predict at what time in future such GW events may become observable again through specific pulsars. Even the GWs from the earliest detected supernova SN185, observed in AD 185, may be observable through observations of perturbed pulses of specific pulsars, (in this case, via pulsars J0900-3144 and pulsar J1858-2216 with perturbed pulsar signal arrival date reaching earth during 2016-2049). The final Section XI will present conclusions and future directions where we will discuss various limitations of these proposals, as well as what specific efforts are needed to make these proposed techniques more effective.

II. QCD PHASE DIAGRAM

This section will discuss salient features of the QCD phase diagram, and possible experimental probes of different regimes of the phase diagram. The earliest known part of the *QCD phase diagram* relates to the liquid/gas transition of nucleonic matter. Indeed, it was the liquid drop model of the nucleus which led Lise Meitner to propose theory of fission [26, 27]. Further structure in this phase diagram emerged from astrophysics, with the notion of neutron superfluidity in the cores of neutron stars [13]. Up to this stage, it would be more appropriate to call it the phase diagram of nucleonic (hadronic) matter. With the discovery of asymptotic freedom, Quantum Chromo Dynamics (QCD) was established as the fundamental theory of strong interactions, with quarks and gluons being the fundamental constituents, and gluons being the mediators of the color force among these constituents. Hadrons were composed of quarks and the nuclear (hadronic) interactions arise as residual interaction from this fundamental color interaction. With the color gauge group $SU(3)$, the QCD Lagrangian is

$$L_{QCD} = -\frac{1}{4}F_{\mu\nu}^a F^{a\mu\nu} + \sum_{\alpha} \bar{\psi}_{\alpha} (i\gamma^{\mu} D_{\mu} - m_{\alpha}) \psi_{\alpha}$$

where $\alpha = u, d, c, s, t, b$ is the flavor index for quarks.

The covariant derivative is

$$D_{\mu}\psi_{\alpha} = (\partial_{\mu} - ig_s T^a A_{\mu}^a) \psi_{\alpha}$$

g_s is the strong interaction coupling constant. ψ_{α} is in the 3-dimensional fundamental representation of color $SU(3)$, with the generators $T^a = \frac{\lambda^a}{2}$, $a = 1, \dots, 8$. A_{μ}^a are the 8 gluon fields and λ^a are the Gell-Mann matrices. The field strength tensor is

$$F_{\mu\nu}^a = \partial_{\mu} A_{\nu}^a - \partial_{\nu} A_{\mu}^a + g_s f^{abc} A_{\mu}^b A_{\nu}^c$$

where f^{abc} are the antisymmetric structure constants for the Lie algebra of $SU(3)$. As isolated quarks are not seen, confinement is an essential part of color interaction. Isolated objects can only be color singlets. Running of the strong interaction coupling constant g_s with energy exhibits the famous *asymptotic freedom*. Writing $\frac{g_s^2}{4\pi} \equiv \alpha_s$,

$$\alpha_s(Q^2) = \frac{4\pi}{(11 - \frac{2n_F}{3}) \ln Q^2/\Lambda^2}$$

Λ is the QCD scale typically taken to be of order 200 MeV. Thus color interaction becomes weaker with large momentum transfer, equivalently at short distances. On the other hand, at large distances, interaction becomes very strong, which is consistent with the notion of color confinement.

With asymptotic freedom, it is but natural to expect that the behavior of strongly interacting matter (system of hadrons) at ultra high temperatures, or ultra-high densities, may show qualitatively different behavior compared to the standard confining hadronic phase. One would expect in such extreme regimes, typical interaction between quarks will be at very large energies/short distances, hence will become much weaker. In the limiting case quarks and gluons should become almost free, hence the notion of an almost ideal gas of quarks and gluons, the quark-gluon plasma (QGP) phase of strongly interacting matter. Extreme limits of temperature are only found in the very early stages of the Universe, while very large baryon densities are expected to arise in cores of neutron stars. These two systems thus provide natural laboratories for the QGP phase of the QCD phase diagram. However, the QGP phase in the early Universe is primarily probed theoretically, with no reasonably direct observable signals expected for the present stage of the Universe. (This is with the present understanding that for very small net baryon densities, the quark-hadron transition is a cross-over. Some time back when the possibility of a first order transition was also there, there were tantalizing possibilities of forming quark nuggets which could be candidates for dark matter [8].) Situation is different with neutron stars which are directly accessible to observations. Observational data available for masses and sizes of neutron stars put strong constraints on the equation of state of the matter inside the neutron star. Detailed information about phases in the interior of a pulsar is provided by observations of pulses, in particular from the pulsar glitches [28]. A remarkable new probe of the neutron star interior in terms of *tidal deformability* became available from the direct detection of gravitational waves by LIGO/Virgo coming from binary neutron star (BNS) merger events [18].

Study of QGP phase, and exploration of QCD phase diagram in general, has acquired new dimensions with

the arrival of relativistic heavy-ion collider experiments (RHICE). Heavy ions (e.g. Lead, Gold, etc.) are accelerated to ultra-relativistic speeds and made to collide, thereby creating a transient ultra hot and dense system of strongly interacting matter. For high enough center of mass energy, the temperatures are expected to be high enough for the creation of a thermalized system of quarks and gluons, the so called quark-gluon plasma (QGP) phase of QCD. These experiments have allowed unprecedented control over the properties of strongly interacting matter created reaching temperatures and densities which were only available so far in cosmos. Controlled experiments have given wealth of knowledge about the system, from thermodynamic properties to transport coefficients, and even allow to study QCD matter in strong external electromagnetic field. The initial goal of these experiments was to find the QGP phase, hence the drive for larger and larger centre of mass energy. Indeed, from Super Proton Synchrotron (SPS) at CERN to Relativistic Heavy-Ion Collider (RHIC) at BNL, USA, and then to Large Hadron Collider (LHC) at CERN, center of mass energy per nucleon-nucleon pair has increased from few tens of GeV at SPS to 200 GeV at RHIC, and 5.36 TeV at LHC for nucleus-nucleus collisions. The temperatures reached at such energies have certainly been high enough to convincingly demonstrate creation of the QGP phase. However, increasing collision energy at the same time leads to lower baryon density for the produced system. This is because of asymptotic freedom of QCD, larger momentum transfer leads to weaker interaction, thereby reducing possibilities of baryon stopping in the produced system. The QGP system produced at ultra high energies, therefore, resembles more closely the QGP phase of the early Universe which also had very small baryon number density.

With these experiments at ultra high energy, creating a QGP system with very small baryon densities, reaching a level of maturity, the attention is now being focused on the other extreme condition, namely very high baryon density regime of QCD matter. QCD matter is also expected to go to QGP phase in this regime, but with different properties. While high temperature low baryon density QGP teaches us about the early Universe, the regime of very high baryon density QGP directly relates to the interior of neutron stars. In fact, it is now realized that the QCD phase diagram has extremely rich structure precisely in this ultra-high baryon density regime. The situation is quite like the phase diagram of water. While at high temperatures we have liquid and gas phases, at ultra low temperatures and densities there are numerous phases of ice which appear. Possibilities of various phases of QCD are illustrated in the QCD phase diagram in Fig.1. Here we show the phase diagram in terms of two most important variables, temperature T and baryon chemical potential μ (representing baryon density). In different situations, one can use other variables such as strangeness chemical potential etc. For theoretical discussions it is also useful to invoke another axis where

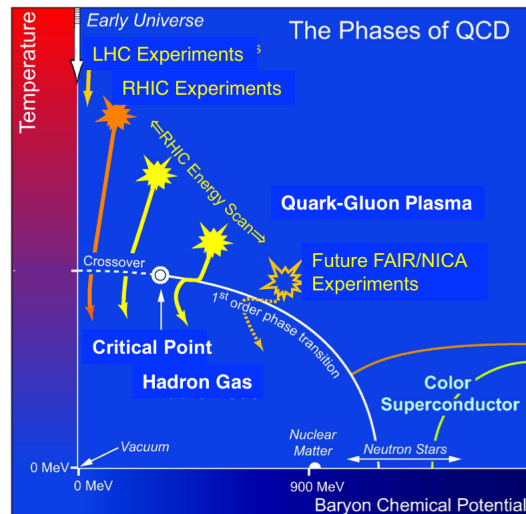


FIG. 1. QCD phase diagram in the T, μ plane (from ref.[29])

quark masses can be varied. This allows for the discussion of various possible phases, and critical points in the phase diagram. We will confine our discussion to the standard 2-d phase diagram as shown in Fig.1, in the T, μ plane.

The phase diagram in Fig.1 shows possible phases in different regions of temperature T and baryon chemical potential μ_B . The figure also shows where different regions of the phase diagram are expected to arise. It is useful to consider two different regimes in the entire phase diagram. One is for relatively low baryon density with baryon chemical potential values less than about 1 GeV, or ultra high temperatures, and the other regime is for much higher values of μ_B and relatively low temperatures.

A. Low baryon density/ultra high temperature regime

There are several regions for separating this regime. First, there are only two phases to discuss here. The hadron gas phase appears at low values of μ_B and relatively low temperatures. Boundary of this phase is denoted by the white curve, part solid, joined to dashed white curve, the joining point denoted as the *critical point*. The solid white curve denotes line of first order transition, which ends at the critical end point where the transition is second order (a continuous phase transition). The dashed line denotes a cross-over transition, which is not a proper phase transition (in the sense that the partition function remains analytic across this boundary). The entire region of the phase diagram outside this boundary, and above the solid yellow line is the second phase, the quark-gluon phase. Importantly, all the present and future planned heavy-ion collision experiments probe this part of the phase diagram only. First

system to discuss here will be the early Universe denoted by the solid white arrow (almost) on the $\mu_B = 0$ line. The temperatures reached in the Universe in its earliest stages can reach close to the Planck temperature ($\sim 10^{19}$ GeV), depending on the inflationary models. The Universe, expanding and cooling from these earliest stages, reaches the quark-hadron transition temperature (where the solid dashed line intersects the T axis). Lattice calculations are under good control for $\mu_B = 0$ case, and give the value of quark-hadron transition temperature to be $T_c = 156$ MeV. This value of temperature is expected to be reached in the early Universe when its age is few tens microseconds. Upto that time, the Universe was filled with a plasma of quarks, gluons, as well as other elementary particles, e.g. leptons, photons. After this time, the Universe undergoes quark-hadron transition, (which is expected to be a smooth cross over from lattice calculations) when quarks and gluons get confined into system of hadrons. As we mentioned, with smooth cross-over the earlier much discussed quark nugget scenario [8] is no more possible. Though, there have been alternate proposals for the formation of quark nuggets which do not depend on the nature of quark-hadron phase transition [30, 31].

The ultra-relativistic collisions at RHIC and LHC, with centre of mass energies ranging from 200 GeV to 5.36 TeV (per nucleon-nucleon collision) lead to a fireball with temperatures well above the quark-hadron transition temperature with relatively low values of μ_B (~ 50 MeV for 200 GeV collision energy). As we mentioned, increasing collision energy leads to smaller values of μ_B due to asymptotic freedom of QCD. For these large values of collision energies, confining forces become irrelevant, so basically the collision is between quarks and gluons (partons) contained in each colliding nuclei. For very large collision energies, partons scatter little, basically the colliding nuclei go through each other. Even with smaller scattering at large energies, the energy available for secondary parton production monotonically increases with collision energies, leading to higher temperatures. But with smaller scattering, proton stopping is less, hence net baryon number of the produced QGP system is monotonically decreasing function of collision energy. (Strong interactions conserve baryon number, so baryon density in the central fireball can only come from the stopping of initial valance quarks of the colliding nuclei.)

It is believed that at these collision energies, the expanding QGP system undergoes quark-hadron transition through the dashed white line in Fig.1, that is the cross-over line. This is with several estimates of the location of the critical point. Though it has not been possible to have a good control over lattice calculations for non-zero μ_B (due to the so called *fermion sign problem*), several techniques have been devised to extend lattice calculations for non-zero μ_B . Recent estimates suggest the location of the critical point to be about ($T \sim 156$ MeV, $\mu_B \sim 65$ MeV) [32]. It should be mentioned that there are strong theoretical arguments for the existence of a

first order transition line at non-zero values of μ_B . These are typically based on various effective field theory models. Combined with the solid knowledge of cross-over transition at $\mu_B = 0$, it automatically follows that the first order line has to end somewhere at a critical end point.

Physics near the critical point (in the critical regime) is dominated by critical fluctuations showing universal properties. Experimental evidence for such fluctuations will give deep insight into this very important part of the QCD phase diagram. With this aim, the beam energy scan program was designed at RHIC, with collision energies as low as 7.7 GeV (thereby creating the QGP system with much higher values of μ_B , hopefully evolving through the critical regime).

One more region deserves mention in this part of the phase diagram, denoted as *Nuclear matter* near $\mu_B = 900$ MeV. There is a short line of first order transition (not shown in Fig.1) which corresponds to liquid-gas transition of nuclear matter. What is more interesting is that at further larger values of μ_B but still within the hadronic phase (so not crossing solid white curve), there is the possibility of nucleonic superfluid phase. It is precisely this superfluid phase, and associated superfluid vortices which are supposed to play crucial role in neutrons stars, especially in relation to the phenomenon of pulsar glitches. We will have details discussion of this phase in the next section.

B. Very high baryon density, low temperature regime, color superconductivity

Discussions relating to this part of the phase diagram have intensified relatively recently. There have been insightful exchanges of ideas between the usual condensed matter physics and this area, which is appropriately being called as *condensed matter physics of strongly interacting matter*. The phases in the part of the phase diagram are typically termed as *color superconducting phases*. Note here that for this part of the QCD phase diagram, we are not including the so called *high baryon density QGP phase* which will be the part above the solid yellow line with very large values of μ_B . Though there will be important differences in the physical properties of QGP with high baryon density from QGP with very low baryon density (and high temperature), they are the same thermodynamic phase, with no phase boundary expected between these two regimes. That is why we included high μ_B QGP phase in the preceding subsection. Discussion below is primary taken from refs.[4–7] which can be consulted for details.

High μ_B with low temperature changes the physics qualitatively giving rise to new thermodynamic phases. The basic physics of these phases lies in the realization that at very high values of μ_B , and relatively low temperatures, the physics will be governed by low energy excitations near the Fermi level. Standard BCS Super-

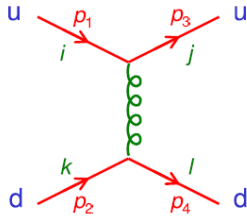


FIG. 2. quark-quark scattering with one-gluon exchange

conductivity has taught us that any attractive interaction between fermions at the Fermi level destabilizes the Fermi level, forming Cooper pairs of fermions. First we note that for the relevant values of chemical potential, only relevant quark flavors are u, d , and s quarks. (We do not discuss here heavier quarks as there is no physical system known where one could reach quark chemical potential high enough so that heavier quarks can play any important role for these condensed phases of QCD.) At ultra high chemical potential, of order 500 MeV for quarks, asymptotic freedom will make perturbative calculations reliable, especially for u and d quarks. Consider scattering of light quarks with one gluon exchange as shown in Fig.2,

Here, $i, j, k, l = 1, 2, 3$ (or r,g,b) refer to colors of u and d quarks. Now we note that the amplitude for this process is the same as that for the QED process $e^- \mu^- \rightarrow e^- \mu^-$ with the replacement of the electromagnetic coupling e by the strong coupling g_s (i.e. replacing α by α_s , and inclusion of the *color factor*),

$$C_F(ik \rightarrow jl) = \frac{1}{4} \lambda_{ij}^a \lambda_{kl}^a \quad (1)$$

quark-quark can combine in two ways, with $3 \times 3 = 3^* + 6$. The color factors for the two representations are, $C_F(3^*) = -2/3$ and $C_F(6) = 1/3$.

As the EM potential between e^- and μ^- is repulsive, the qq potential is attractive in the 3^* channel, and repulsive in the 6 channel. BCS pairing of quarks in the 3^* channel leads to the *color superconducting phase*. Depending on the relative masses of the quarks forming the condensate, different phases are possible.

Color-Flavor Locked (CFL) phase:

With color antisymmetric (3^* channel), spin antisymmetric (for 1S_0 pairing), we conclude that the condensate should have flavor antisymmetric. For very high chemical potential it may be reasonable to treat all three quarks

(u, d, s) as massless. Condensate for this most symmetric case, (with 1S_0 spin pairing) will have the following structure

$$\langle q_i^\alpha q_j^\beta \rangle \sim \Delta_{CFL} (\delta_i^\alpha \delta_j^\beta - \delta_j^\alpha \delta_i^\beta) = \Delta_{CFL} \epsilon^{\alpha\beta n} \epsilon_{ijn} \quad (2)$$

where $\alpha\beta$ are flavor indices and ij are color indices. Note that the condensate is invariant under equal and opposite rotations of color and (vector) flavor. Hence, it leads to the following spontaneous symmetry breaking

$$SU(3)_{Color} \times SU(3)_L \times SU(3)_R \times U(1)_B \rightarrow SU(3)_{C+L+R} \times Z_2 \quad (3)$$

Thus color symmetry of QCD $SU(3)_C$ is spontaneously broken. Three flavor Chiral symmetry is also spontaneously broken. Interestingly, QGP phase restores the chiral symmetry (at least for $\mu_B = 0$ case). Here, at large μ_B also, we expect chiral symmetry restoration in the *high density QGP phase* which occurs at higher temperatures. But at low temperatures, high μ_B quark-gluon phase breaks the chiral symmetry spontaneously. We will discuss the situation with chiral symmetry further below.

Spontaneous Breaking of $SU(3)$ color symmetry implies that all gluons become massive, (so there are no long range color forces even in this deconfined phase), hence the name *Color superconductor*. We mention here that the role of photon in this broken phase is played by the usual photon with a small admixture of gluon, see [4] for details. Also, note that spontaneous breaking of chiral symmetry, here is not by a color neutral condensate (as for the $\mu_B = 0$ case, but by a colored condensate. This implies multiplets of colored hadrons, (and also colored Skyrmions),

2SC Pairing:

For Cooper pairing of 2 light quarks, we get the so called *2SC phase*. This breaks color group $SU(3)_C$ to color $SU(2)$. In this phase, 5 out of 8 gluons become massive.

Crystalline Color Superconducting phase:

This phase is similar to the so called Larkin-Ovchinnikov-Fulde-Ferrell (LOFF) phase in condensed matter systems: When chemical potential is not very large compared to the strange quark mass, then difference between u, d quark masses and s quark mass becomes significant. In that case Cooper pairing of different quarks (having different Fermi momenta), leads to spatial modulation of the order parameter. This implies spontaneous breaking of spatial translations (and rotation) symmetries.

We are only giving brief details of various phases here, just to give an idea of the richness of the QCD phase diagram in different regimes. There are excellent references available in literature, we have listed some here in refs.[4-7]. We end this section with brief discussion the important subject of chiral symmetry in QCD.

C. Chiral Symmetry in QCD

We here briefly recall the notion of chiral symmetry in QCD. For details, literature can be consulted, e.g. ref. [33]. Note that we have been using the term *quark-hadron transition* in the above discussion. This term can have two meanings. One is the confinement-deconfinement (C-D) transition where a system of hadrons, (with quarks/gluons being confined inside hadrons) makes a transition to the deconfined phase of a plasma of quarks and gluons. The other meaning can refer to the chiral transition. For 2 massless flavors, QCD Lagrangian has exact $SU(2)_L \times SU(2)_R$ symmetry, called as 2-flavor chiral symmetry, which corresponds to independent transformations of left and right components of u and d quarks. Hadron spectrum does not show any such doubling of mass spectrum, but it does show multiplet structure of $SU(2)_{isospin}$. This leads to the conclusion that the chiral symmetry $SU(2)_L \times SU(2)_R$ is spontaneously broken to the diagonal subgroup $SU(2)_{isospin}$, with pions as the Goldstone bosons. For three massless flavors, all $SU(2)$ groups should be replaced by $SU(3)$ groups, leading to 3-flavor chiral symmetry breaking. Of course, quarks are not massless, this leads to explicit breaking of chiral symmetry, leading to small masses for the Goldstone bosons, and contributing to mass differences within the multiplets. The explicit symmetry breaking being relatively small, especially for the 2-flavor case, the notion of chiral symmetry in QCD has been immensely useful, especially in constructing effective field theory models which capture physics at low energy scale. Chiral sigma models, Nambu-Jona-Lasinio (NJL) models etc. are all based on the notion of chiral symmetry breaking and have been the only tools for discussions of QCD phase diagram at high baryon densities.

It is believed that chiral symmetry transition and confinement-deconfinement (C-D) transition are the same. Lattice results support this idea (though at times there are differing results also). Conceptually, these two transitions are completely different. Indeed, different order parameters characterize these two transitions, with expectation value of the Polyakov loop characterizing the C-D phase, and the $\bar{\psi}\psi$ condensate characterizing the chiral transition (ψ being the quark field). We will have discussion of some of these (especially the Polyakov loop condensate) later in Section VI. The conceptual difference between these two transitions becomes clear when we consider high μ_B phases, in particular the color superconducting phases. These phases appear in the regime where inter-quark separation is so small that confining forces are irrelevant. This is like a plasma of deconfined quarks and gluons, but not the usual QGP phase as here thermal effects are insignificant compared to the quantum statistics effects. Thus, we have chiral symmetry breaking here (as discussed above for the *CFL* phase), even though we have a system of deconfined quarks and gluons. Note that although we have massive gluons here, there is no relevance of color singlet objects here. Indeed,

as mentioned above, we expect colored hadrons here arising from the chiral symmetry breaking via a colored diquark condensate.

III. NEUTRON STARS

This section will discuss basic physics of neutron stars, including the superfluid phase in its interior as well as the possibility of exotic QCD phases in the inner core. We will also briefly discuss how the recent gravitational wave detections have allowed the probe on NS interior properties.

Basics of a neutron star : The existence of neutron stars as one of the possible end states of massive stars was predicted by Walter Baade and Fritz Zwicky in 1933 [34], a long time before the discovery of the pulsating neutron star (*little green man*) in late 1967 [35]. Neutron stars are the remnants of the supernova explosion of supergiant stars of mass in the range $10 M_\odot - 20 M_\odot$. During its formation, gravity squeezes the matter to achieve extremely high baryon density. Gravitational collapse is counterbalanced by the neutron degeneracy pressure (along with repulsive nuclear forces) leading to the formation of a stable neutron star. The radius (R) of a neutron star lies in the range (10 - 14) km with mass in the range $1.1 M_\odot - 2.1 M_\odot$. Thus the average mass density is of the order of nuclear matter's saturation density $\rho_0 = 2.8 \times 10^{14} \text{ g cm}^{-3}$. The discovery of the neutron star put the discussions of such compact astrophysical objects on deep footing, with the realization that it provides the opportunity for testing exciting physics at a high baryon density regime that cannot be tested otherwise by terrestrial experiments. However, with the opportunity, new theoretical challenges arise, of understanding the properties of dense interior materials, the inner core in particular, and relating these properties to various testable observables.

There have been continuous efforts towards a theoretical understanding of the internal structure of neutron stars keeping in view its astrophysical implications and observational constraints. These include the mass-radius relations, the moments of inertia (MI) of the star (including the fractional contribution of the solid crust and superfluid/superconductor components), the extent of rigidity of the outer crust, and the deformation from the sphericity etc. The above quantities, in turn, determine the frequency of pulsar's free precession, glitch size in the context of various pulsar glitch models (crustquake, superfluid-vortex model etc.), or the feasibility of GW emission etc.

The standard approach of constructing a model of neutron star's internal structure is to implement hydrostatic equilibrium of a gravitating fluid system, resulting in the well known Tolman-Oppenheimer-Volkoff (TOV) equa-

tions [36, 37] ($c = 1 = G$),

$$\frac{dP(r)}{dr} = -\frac{(P + \rho)(M + 4\pi r^3 P)}{r(r - 2M)}; \quad (4)$$

$$\frac{dM(r)}{dr} = 4\pi\rho(r)r^2. \quad (5)$$

The solutions of the above set of equations provide the density profile $\rho(r)$, including the mass and the radius of the neutron star, provided the equation of state (EOS) $P = P(\rho)$ and the central density $\rho(0)$ are supplied. The above procedure thus produces a neutron star structure model for a fixed value of central density, which finally determines various physical parameters, such as the mass, radius, moment of inertia, etc., of the star. However, the main challenge lies in providing the EOS, the most critical input for solving the Eqs. (4,5). Although the EOS of the outer crust and, to some extent, the inner crust are known [38], the first principle calculations of the many-body QCD interaction relevant to the inner core are unknown. Thus, one has to resort to phenomenological models for extracting the EOS for the core region. One can then use the experimental measured values of various physical parameters to test the predictions based on constructed stellar models. For most practical calculations, one uses a set of canonical values $M = 1.4 M_{\odot}$, $R = 10$ km, and $MI = 10^{45}$ g cm². For the above set of values, and from the observations of various pulsar events, such as glitches (to be discussed later), one broadly takes the neutron star's internal structure as shown in Fig. 3.

Observation of glitches in the rotation of young pulsars indicates a solid crust containing $\geq 1.4\%$ of total MI [39], the outer layer of which consists of crystalline solid iron nuclei and a sea of degenerate electrons with mass density $\rho \simeq 10^6$ g cm⁻³. Going deeper into the inner crust region, as the density increases from $\rho \simeq 10^{11}$ g cm⁻³ onward, protons and electrons start combining to form neutrons for creating neutron-rich nuclei. Eventually, it becomes energetically favorable for the neutrons dripping out of the nuclei and forming a sea of free (unbounded) neutrons. A few hundred meters thick inner crust region with the density ranging from approximately 10^{11} g cm⁻³ to 10^{14} g cm⁻³ plays a crucial role in the theory of glitches. There is a strong belief, supported by glitch observations, that a significant fraction of free neutrons in this region (see Fig. 3) are in a 1S_0 neutron superfluid state. Further deeper, below the inner crust region, a more favorable 3P_2 neutron superfluid state is believed to co-exist with a 1S_0 proton superconductor.

The composition of the inner core is highly speculative. The states of matter at the high pressures in the deep interior can form various hadronic states, such as hyperons, condensed-pions etc. The central region of the neutron star can also accommodate different QCD phases, such as QGP, CFL, 2SC, etc. The core centre can become quite mysterious for massive neutron stars. One needs well

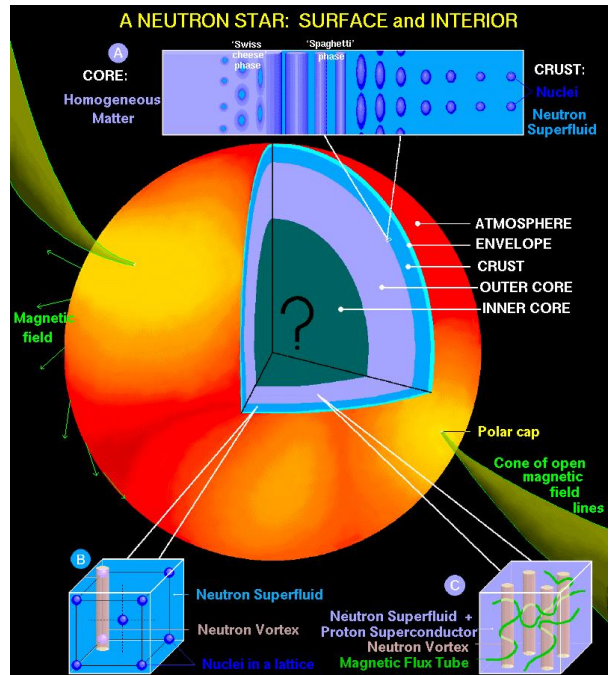


FIG. 3. The expected internal structure of a neutron star. Credit : Dany P Page (<https://phys.org/news/2015-09-neutron-star.html>).

defined signatures that can be tested to confirm possibilities of any such phases which remains an important theoretical challenge.

We will be discussing later various proposals and observational techniques for probing physics of pulsar interior. But, it seems most appropriate to close this section with a discussion of a truly exciting recent development towards probing neutron star interior. This is the direct detection of gravitational waves by LIGO/Virgo which, for GWs originating from a BNS merger allows to put observational constraints on deformation of neutron stars during last stages of coalescence, thereby directly probing the stage of matter inside the neutron star.

Probing NS interior with direct detection of gravitational waves from BNS merger

Possibly the most important advancement in experimental General Relativity in recent years has been the direct detection of gravitational waves by LIGO and Virgo coming from distant events of binary black hole mergers and subsequently, binary neutron star mergers. Black hole merger events allow the possibility of directly probing the dynamics of intense gravity regime of near horizon regions of black holes by analysis of the GW waveform corresponding to the near coalescence regime of black

holes. Similarly, for binary neutron star merger events, GW waveform contains information about strong tidal deformations towards the end of spiral-in of the neutron stars, when separation between the two neutron stars approaches neutron star size. In such regime, the coalescence is accelerated by a quadrupolar deformation of NS by the tidal field of the companion NS. Indeed, GW waveform observations have been used [18] to put constraints on the dimensionless tidal deformability $\Lambda = \frac{2}{3}K_2R^5/M^5$ (in gravitational units with $G = c = 1$) where k_2 is called the second Love number. (Λ is related to the tidal deformability λ discussed later in Sec. IX, by $\Lambda = \lambda/M^5$.) value of k_2 and hence the tidal deformability depends on the equation of state of NS matter. GW observations thus provide a completely independent probe of the equation of state of NS matter, which is usually constrained by mass-radius relationship of neutron stars. Direct observation of source identification for BNS mergers by resulting electromagnetic radiation (which would be absent for black hole mergers) has started the new chapter of multimessenger astronomy in our exploration of cosmos. With a range of observations, from gravitational waves, to electromagnetic radiation in a range of energies, along with the possibility of neutrino bursts from such BNS merger events will jointly give a powerful probe of the structure and property of neutron stars.

IV. PULSARS

This section will be devoted to pulsars recalling the extreme accuracy of pulsar timing observations. We will also briefly discuss here the first (indirect) detection of gravitational waves (GWs) by pulsar observations, as well as ongoing attempts of pulsar timing arrays for detection of ultra low frequency GWs.

Pulsars Timing : The atomic clock-like stability of pulsar rotation period allows one, through monitoring of the pulsar rotation, to study a rich variety of phenomenon affecting the propagation of pulses while reaching earth. Most applications of pulsars involve a powerful technique known as the pulsar timing. Measurement of a sequence of time of arrival (ToA) of pulses over intervals ranging from hours to decades is the basis of pulsar timing [40]. These ToAs are first transferred, normally to the solar-system barycentre, to remove the effects of rotation and orbital motion of the Earth. The amount of useful information that can be extracted critically depends on the precision at which the pulse arrival times are measured. In order to understand the pulsar timing, we will take the example of isolated pulsars and describe the rotation in the pulsar's comoving frame. For an isolated pulsar, one can express the spin frequency ν (or time period P) in a Taylor series about some reference epoch t_0 [40]

$$\nu(t) = \nu_0 + \dot{\nu}(t - t_0) + \frac{\ddot{\nu}(t - t_0)^2}{2} + \dots \quad (6)$$

Where $\nu_0 = \nu(t_0)$ is the pulsar's spin frequency at t_0 and $\dot{\nu}, \ddot{\nu}, \dots$ are the higher order time derivatives of ν to be evaluated at t_0 . These parameters are associated with some physical process, knowledge of which provides valuable information about the underline process. For a normal (i.e., rotation-powered) pulsar, the period P (~ 0.3 s - 3 s) and its first derivative \dot{P} ($\sim 10^{-15}$ s s $^{-1}$) are observed with high accuracy through timing measurements. These parameters capture the spin-down history of the isolated pulsar. On the other hand, the millisecond pulsars (MSP) have the most exotic applications, including the detection of low-frequency gravitational waves (see below) because of their extreme stability in their periodicity ($P \sim 3$ ms with $\dot{P} \sim 10^{-20}$ s s $^{-1}$) compared to the normal pulsar.

Indirect detection of GWs : The celebrated discovery of the pulsar PSR B1913+16 in binary star system by Russell Hulse and Joseph Taylor in 1974 [15] using the data from the Arecibo radio telescope opened up the possibilities for the study of relativistic gravity in moderately strong field regime. The above discovery provided the first indirect quantitative confirmation test in favor of the existence of gravitational waves within the framework of Einstein's theory of gravity [16, 41, 42]. The Hulse-Taylor pulsar (PSR B1913+16) is a binary star system composed of a pulsar of mass $\simeq 1.44 M_\odot$ and the silent companion neutron star of mass $\simeq 1.39 M_\odot$ [43], moving around in elliptical orbits about their center of mass. As per Einstein's theory of gravity, the orbital period of this binary system is expected to decay with time. The heartening agreement between the observed data with the theoretical prediction (see Fig. 4) not only provided conclusive evidence for the existence of gravitational waves; it laid the foundation for the belief of the possibility of *direct* detection of GWs. The remarkable first-ever direct detection of GWs in 2015 by LIGO [17], arising from a binary black hole merger, fulfills that belief and opens a new era in gravitational wave astronomy. Since then, there have been quite a few significant detections of GWs. The peak strain amplitude (h_0) for all these detections has been in the range $10^{-21} - 10^{-22}$.

There were several theoretical studies [19, 44–46], where the authors suggested that isolated pulsars can be a potential source of GWs. A few other neutron star activities, such as the neutron star flaring, the formation of hyper-massive NS following binary coalescence, etc., are capable of exciting quasi-normal modes of a pulsar, resulting in the GWs emission. The primary purpose of such studies is to probe the internal structure of the pulsars. Hopefully, the more sensitive ground-based advanced detectors, namely, aLIGO, VIRGO, Einstein Telescope (ET) etc., will be able to measure the gravitational waves produced by isolated pulsars shortly and answer a few questions on pulsar physics. In fact, with the above purpose, even before the direct detection of GWs, there were a few attempts for GWs searches from

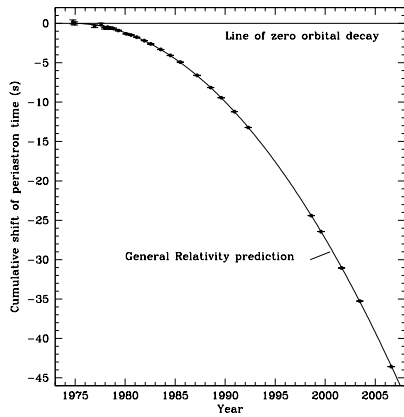


FIG. 4. The shift in the periastron passage of the binary pulsar PSR B1913+16 with time, caused by gravitational radiation. Figure taken from Ref. [43]

isolated pulsars. The GWs associated with the timing glitch in the Vela pulsar in August 2006 [47] was one among those searches worth mentioning. The observed timing noise, i.e., glitch, can be one such activity that can excite quasi-normal modes in the pulsar and cause GWs. Although the searches during the August 2006 Vela pulsar timing glitch produced no detectable GWs [17], with the improving sensitivity of advanced detectors, continuous attempts in this direction may produce more conclusive results shortly.

Pulsar Timing Array (PTA) : Pulsar timing arrays are the GW detector setups provided by nature itself, in the form of a population of highly stable millisecond pulsars, with timing accuracies of ~ 10 ns over several years, with arm lengths of galactic scale. They are sensitive to much lower frequencies than ground-based instruments. With precise pulsar timing, an array of pulsars could detect extremely low-frequency sources with typical frequencies less than 10^{-6} Hz. The origins of GWs with such low frequency can be supermassive black hole mergers with masses in the range $(10^9 - 10^{10}) M_{\odot}$, the stochastic background of GWs arising from cosmological phase transition during the early stages of the Universe, or otherwise, or more exotic objects such as cosmic strings. The basic principle is that the set of stable MSPs serves as an array of clocks whose *time*, as observed on earth, would be modulated by gravitational waves passing through the space between MSP and Earth. With observations of many pulsars, phenomena which affect all pulsar periods in a correlated way can be separated from phenomena which affect different pulsars differently. For example, a stochastic gravitational wave background can be separated from errors in the time standard because of their different dependence on pulsar sky position. For example, clock errors will lead to all pulsars having the same Time of Arrival (TOA) variations (monopole signature), solar-system ephemeris errors will lead to a dipole signature. In contrast, gravitational waves will lead to a

quadrupole signature. These effects can be separated if one has sufficient number of widely distributed pulsars. With this purpose, there is a worldwide effort to search for and observe the set of stable millisecond pulsars for detecting gravitational waves through pulse modulation. There are four current efforts in this direction, operating under the joint umbrella of the International Pulsar Timing Array (IPTA [48]); North American Nanohertz Observatory for Gravitational Waves (NANOGrav) in the USA, the Parkes Pulsar Timing Array (PPTA) in Australia, the European Pulsar Timing Array (EPTA), and the Indian Pulsar Timing Array Project (InPTA). IPTA aims to construct the most sensitive low-frequency gravitational wave detector, which can be achieved through sharing resources among the stakeholders and creating combined pulsar timing data sets. The current sensitivity of the experiments is exciting from the perspective of the potential detection of GWs through PTA.

V. OBSERVATIONAL ASPECTS OF NEUTRON STAR INTERIORS

Here we will discuss various proposals from the literature for possible observational signatures of various phases in NS interiors. Among these, glitches take a prominent role as well established signals for the existence of the superfluid phase in NS interior. We will discuss here difficulty of this explanation in accounting for relatively recent observations of anti-glitches. We will also discuss various proposals for detection of the exotic color superconducting phases of QCD in NS interior.

Pulsar glitches : Pulsars are magnetized rotating neutron stars that emits periodic short pulses of electromagnetic radiation with periods between 1.4 ms - 0.3 s. The non-alignment of the rotation axis with the magnetic axis causes the light-house-like appearance of the pulses to the observer at Earth. Amid the pulsars' extraordinarily stable rotational frequency, many pulsars show sudden spin-up events (glitches) followed by a period of slow recovery.

Since the discovery of the first glitch in the Vela pulsar [49], many glitches have been observed and reported to date [50]. A typical glitch pattern is shown in Fig. 5. The fractional change of rotational frequency, i.e., the glitch size $(\Delta\Omega/\Omega)$ lies in the range $10^{-11} - 10^{-5}$ with an average inter-glitch time of a few months to a few years. The pulsar recovers from weeks to months to a period close to the pre-glitch value. The oldest theoretical model for pulsar glitches [51], namely, the crustquake model, assumes the existence of a deformed solid crust of a pulsar. The oblateness can be characterized by the parameter $\epsilon = \frac{I_{zz} - I_{xx}}{I_0}$. Where I_{zz} , I_{xx} and I_0 are the moment of inertia about the z-axis (rotation axis), x-axis, and the spherical star, respectively [52]. The sudden decrease of oblateness $\Delta\epsilon$ decreases the MI, resulting in a spin-up event (following angular momentum conservation), i.e., $\frac{\Delta\Omega}{\Omega} = -\frac{\Delta I}{I_0} = \Delta\epsilon$. It was immediately realized [52]

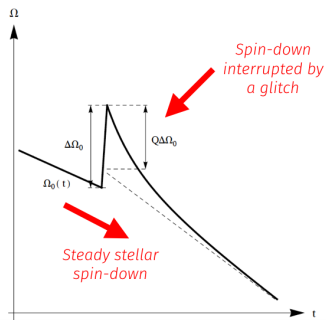


FIG. 5. A schematic representation of a typical glitch pattern of a pulsar. Here Q is the recovery fraction, which measures the part of $\Delta\Omega$ which decays. The post-glitch recovery time scale typically ranges from a few days to weeks. (Taken from: <http://hdl.handle.net/11343/36537>.)

that inter-glitch time being proportional to $\Delta\epsilon$, successive large-size glitches need longer waiting periods. Thus, crustquake might be responsible for producing smaller Crab-like glitches $\Delta\Omega/\Omega \simeq 10^{-8}$; the model is incompatible with Vela-like large-size glitches $\Delta\Omega/\Omega \simeq 10^{-6}$.

Anderson & Itoh proposed the most popular superfluid-vortex model in 1975 [28]. The model assumes the existence of neutron superfluidity in the inner crust, with the core being in a superfluidity/superconducting state. Interestingly, superfluidity in a neutron star was hypothesized [53] a long time before the above-proposed glitch model. The basic idea of the vortex model is that the vortices (spinning neutron star causes an array of quantized vortices for stability) act as an angular momentum reservoir while being pinned to the nuclear sites [46, 54–56]. As the neutron star slows down due to radiation loss, differential angular velocity $\delta\Omega$ between the inner crust superfluid and the rest (crust+core) is built until it reaches a critical value $(\delta\Omega)_c$. Once the Magnus force overcomes the pinning force, just above $(\delta\Omega)_c$, many vortices ($\sim 10^{18}$) are released from the pinning site and share the excess angular momentum to the rigid crust-core co-rotating system, causing the pulsar to spin-up. The vortex model not only can account for large-size Vela-like glitches ($\sim 10^{-6}$), the long-relaxation time scale (weeks to months) associated with the post-glitch recovery phase also arises naturally in this picture, thus providing indirect evidence of superfluidity in the interior [57]. In this context we mention that an interesting spin-down event was observed a decade earlier in the magnetar 1E 2259+586. As per the report [58], X-ray timing observation [59] of the magnetar clearly shows an anti-glitch. Evidence for anti-glitches in the X-ray pulsar NGC 300 ULX-1 is also reported recently [60]. Such events challenge the standard glitch theory and suggest the need for rethinking this issue [19].

Mesonic condensate phases

It has been suggested that at high baryon densities in the core of neutron stars, apart from the neutrons and

protons, various mesonic condensates may form. Formation of pion condensate has been suggested, (see, e.g. [61–63]) and it has been argued that it may lead to significant modification of equation of state. Kaon condensates have also been considered and its effects on softening the equation of state, hence constraining the maximum mass of neutron stars has been discussed [64, 65]. These condensates may also affect the cooling rate of the neutron star. Along with such condensates, dominant presence of hyperons in the NS interior has been discussed, and constraints on maximum mass of NS have been derived [66]. Effect of hyperons on the possibility of pion condensates has been discussed in [67] and it has been argued that with hyperons, it is unlikely that s-wave pion condensate could form in the NS interior.

Quark matter core:

At high baryon densities, the core of the neutron star is likely to convert to quark matter. With the outer regions being in the hadronic phase, there will be a phase boundary separating the quark core from the hadronic region. With quark matter equation of state for the core, the mass and size relationship of the neutron star is affected [68] which can be probed by observations, e.g. using thermonuclear X-ray bursts from matter accretion on NS surface in binary systems [69]. The compactness of the neutron star (M/R) is directly probed by the tidal deformability from gravitational wave detection from binary neutron star mergers. Possibility of strange quark matter in the high density core of neutron star has been discussed where three-flavor quark matter is assumed more stable than nuclear matter at low density [8–12]. The composition of the core also affects the cooling of neutron star by neutrino emission.

Color superconducting phases : The quark matter core itself can have very rich phase structure at very high baryon densities, as we discussed earlier in the Section II. In the QCD phase diagram, we have observed that the QCD theory allows the appearance of various exotic phases at the low-temperature (T) and very high baryon chemical potential (μ_B) regime. The neutron star’s core can provide such conditions to accommodate those phases. One such phase, the color superconducting phase, may arise due to spontaneously broken $SU(3)_C$ color and chiral symmetry for three light quark flavors (u, d & s). For two light quarks, color group $SU(3)_C$ is broken down to color $SU(2)_C$ causing the so-called $2SC$ phase. Observational signatures of these phases have been discussed in the literature [5, 6]. For example, central core with CFL phase leads to suppressed cooling by neutrino emission, and also has smaller specific heat. Thus the total heat capacity and neutrino emission of NS with CFL core will be dominated by outer layer which are in the standard nucleonic phase. For somewhat lower baryon densities, crystalline color superconductivity may arise in the NS core. It has been suggested that the rigidity of such a phase (possibly with suitably misaligned magnetic field from the rotation axis) will lead to non-zero quadrupole moment [5]. This will be a sig-

nificant source of gravitational waves, which can be observationally constrained with the present generation of gravitational wave detectors.

With the realization that many of these possible signatures of the exotic QCD phases are subject to model uncertainties, an attempt was made by some of us in [19] that the above symmetric breaking phase transitions may cause density fluctuations in the core through the formation of topological defects, leading to a transient change of MI tensors components. It was shown in Ref. [19] that the change of diagonal components of the MI tensor may lead to the change of the spin frequency of the pulsars and may be responsible for glitches and/or anti-glitches. As the fluctuations are random, there is a possibility of the generation of quadrupole moment leading to the emission of GWs. Development of the non-zero MI tensor's diagonal components may also lead to modulations of pulse profile [21]. Contrary to the above proposal, there was also a view in Ref. [70] that the color superconducting phase associated with the three light flavors might not exist. The authors also claimed that two-flavor color superconductivity (2SC) might be marginally inconsistent with pulsar data.

A. Possibility of ultra-high baryon densities in matter collapsing to a black hole

Neutron star core is generally believed to be the place where the highest baryon density can be achieved in nature. Thus the possibility of quark matter and other exotic QCD phases are usually discussed in that context (here we include quark star, strange star etc. in the same category). These are supposed to be equilibrium configurations achieved by using suitable equation of state for the interior. What happens when such compact objects accrete matter? Beyond a limit, the equilibrium is broken and the collapse to black hole occurs. Typically, the collapse is very rapid, occurring in milliseconds for a typical stellar mass object. During this collapse, density keeps increasing, while an event horizon starts forming near the centre, which grows outwards. It is reasonable to expect that during this dynamical evolution, density will be significantly larger than the initial density of the equilibrium configuration. Even before the event horizon forms at the centre, the central density will keep growing, and after the formation of horizon, the region outside it will also have large density before it gets engulfed by the growing horizon. For a naive estimate, consider a stellar-mass black hole of mass, say, $2 M_{\odot}$ (approximately the upper mass limit of a neutron star, though there is still a theoretical uncertainty in estimates of this limiting mass). The Schwarzschild radius $r_s = 2GM/c^2$ of this type of black hole is about 6 km. Thus it is possible that baryon densities in matter ρ_{bh} collapsing to a black hole may become about $(2/1.4)(10/6)^3 \simeq 5$ times larger than the average mass density of a canonical neutron star of mass $1.4 M_{\odot}$ and radius 10 km. Thus, such collapsing

proto black holes may provide possibly the highest possible densities available in nature, larger than any compact equilibrium stars. This should be most optimistic place for looking for extreme exotic QCD phases, such as CFL phase which require very high baryon densities. Even though such high densities will last for a very short times, less than a millisecond, it is a very large time for the QCD processes which occur at time scale of fm/c. Thus observational signals from phase transitions to different high density QCD phases may be detectable when such collapse occurs. Possibility of transition to quark matter core in core-collapse supernova simulations was discussed in [71]. What we are proposing is that even more exotic QCD phases requiring extreme baryon densities may show up transiently in matter collapsing to black hole, for suitable masses of collapsing object. Numerical simulations of neutron stars accreting matter and collapsing to black hole show that central density can significantly increase even before event horizon forms at the centre [72–74]. The signatures from such collapse should be very unique, as there will be a succession of phase transitions to various high baryon density QCD phases, all occurring within a time span of order milliseconds. Apart from signaling exotic QCD phases, it can provide unique signature of such a gravitational collapse to black holes.

VI. DETECTING PHASE TRANSITION OCCURRING INSIDE A PULSAR

Here we will discuss observational implications of phase transitions occurring inside a pulsar, in particular, on the nature of its pulses. The consequences of phase transition (for example from nuclear matter to QGP) occurring in the core of a neutron star on its rotational dynamics has been discussed in [24, 25]. Basic physics of their model is that as pulsar rotation slows down due to radiation braking, the density of the core steadily increases (with reduction of centrifugal force). If the density was initially below the critical density of the pulsar core (corresponding to a phase transition), then at some stage central density crosses the critical value leading to phase transition. It is assumed that as the high density core grows in size (slowly, over the time scale of millions of years), it continuously converts to the high density QGP phase (even when the transition is of first order). The dependence of pressure on density will determine the manner in which the phase transition will affect the moment of inertia of the neutron star, hence the angular velocity of the star. It was emphasized in these works that the quantity of special interest is the *breaking index* defined as $n(\Omega) \equiv \frac{\dot{\Omega}}{\Omega^2}$. It is argued that while usually $n(\Omega)$ will be equal to the intrinsic index n of the energy-loss mechanism (with the energy loss $dE/dt = \frac{d}{dt}(\frac{1}{2}I\Omega^2) = -C\Omega^{n+1}$), during phase transitions, it can differ markedly from this value, possibly even by orders of magnitude. Thus, even if the changes in moment of inertia, and hence the spin rate

changes are not directly observable (due to very large time scale), breaking index may provide a more promising signal for phase transitions occurring inside pulsars.

The discussions in refs. [24, 25] primarily focused on the change in the equation of state during the phase transition. Main consequence of the phase transition was thus related to change in the diagonal components of the moment of inertia tensor affecting the spin rate of the neutron star. However, all phase transitions necessarily produce density fluctuations. In fact, a rich spectrum of physics is encoded in the distribution of density fluctuations relating to the nature of phase transition (first order, second order), and in particular the symmetry breaking pattern (if any) associated with the phase transition. Density fluctuations perturb entire moment of inertia tensor, including its off-diagonal components. This was discussed by some of us in [19, 20] for the situation when phase transition occurs rapidly in a large core of neutron star. It was pointed out that as phase transitions induced density fluctuations modify the entire moment of inertial tensor of the pulsar, the resulting off-diagonal components will lead to wobbling of star (in addition to any previously present) which will induces modulations of the pulse profile. Thus, it was argued that the detailed modification of the pulses carries the information of statistical nature of density fluctuations, and hence the precise nature of phase transition occurring inside the NS interior. An important aspect of this model is that it predicts that off-diagonal components of the MI tensor components necessarily become non-zero along with its diagonal components, with all perturbations being of similar order, due to statistical nature of the phase transition induced density fluctuations. Thus, in this model, spin rate changes will be necessarily associated with the modulations of pulse profile. This can be used to test this model for any observed pulse modifications, as if spin rate changes occur due to de-pinning of vortices, then dominant changes only occur in the diagonal components of the MI tensor (as all vortices are aligned along the rotation axis).

A. Effects of density fluctuations

The earlier discussions in refs. [24, 25] related to a scenario of slow transition as applicable for slowly evolving star (e.g. by accretion), with a transition which is either a weak first order, or a second order, (or a crossover). For a strongly first order transition a different possibility arises as discussed in [19, 20]. Strong supercooling can lead to a highly suppressed nucleation rate, so that no bubble nucleation occurs for a very long time. The transition can then occur suddenly, possibly due to some inhomogeneity, after the supercritical core becomes macroscopic in size. The phase transition thus occurs rapidly over a macroscopically large core. This scenario would be quite similar to the one discussed by Witten [8] where a very low nucleation rate could lead to macroscopic length

scales, of order of meters, for bubble nucleations for the quark-hadron transition where the typical length scale would be of order fm. (The discussion in [8] assumed a first order transition. With lattice results, now one knows that for very low baryonic chemical potential the quark-hadron transition is a cross-over). Rapid phase transition occurring over a large core can occur for in other situations also, for example during early hot stages of the neutron star undergoing rapid cooling.) The discussion in ref. [19, 20] related to a general such situation and argued that, along with the expected change in the moment of inertia, and hence the spin rate, (which could be directly observable), density fluctuations will be produced in the entire large core region undergoing this rapid phase transition. This will then affect off-diagonal MI components and hence induce wobbling of the neutron star.

The situation considered in ref. [19, 20] related to the case when phase transition induced spin rate remains small, (say, within the range set by observations of glitches), and determined the effects of density fluctuations on the MI tensor. In a simplified, two density picture of the phase transition occurring in the NS, it is assumed that the phase transition converts the core of radius R_0 to the new phase with density ρ_2 , while the rest of NS remains in the old phase with density ρ_1 . The resulting fractional change in the moment of inertia [25] is

$$\frac{\Delta I}{I} \approx \frac{5}{3} \left(\frac{\rho_2}{\rho_1} - 1 \right) \frac{R_0^3}{R^3} \quad (7)$$

Where R is the radius of the star (taken to be spherical) in absence of the dense core. If we consider the possibility that phase transitions could have occurred in the pulsars which have been regularly monitored, then observations of glitches can be used to constrain the size of the core undergoing phase transition. One would then constrain the largest fractional change of moment of inertia to be less than 10^{-5} , relating to strongest glitches observed so far. Various phase transition cases can then be considered. For example, a sample value of change in density due to phase transition can be taken to be about 30% (which could be appropriate for QCD transition where density change can be of order one). This will constrain the value of R_0 to be less than about $300m$ (taking $R = 10$ km). Another important case is that of superfluid transition where the density change can be taken to be of order of the superfluid condensation energy density ($\approx 0.1 MeV/fm^3$) [13, 75]. In this case, glitch constraint will implying that R_0 can be as large as 5 km.

With the size of the core undergoing phase transition being constrained, one can then discuss effects of density fluctuations occurring in this core [19, 20]. First it is useful to get generic estimates which depend simply on the nature of phase transition. First, we focus on density fluctuations due to the nucleation of bubbles. As

discussed above, for a strong first-order case, a core of size a few hundred meters (or larger) can undergo rapid phase transition. However, in general, the core region will be expected to have minute nonuniformities, even of purely statistical origin, so that one can consider a situation where many bubbles may nucleate in different parts of the supercritical core. The bubbles nucleated with a critical size of the order of tens of fm , will expand and coalesce. At the time of coalescence, the supercritical core region will consist of close packing of bubbles of the new phase, embedded in the old phase. We carried out simulation of random spherical bubble nucleation of radius r_0 (at the coalescence stage) filling up a spherical core of radius $R_0 = 300m$. The density change in bubble nucleation is taken to $\sim 160 \text{ MeV}/\text{fm}^3$, as appropriate for the QCD transition. We find fractional change in moment of inertia $\Delta I/I \approx 4 \times 10^{-8}$ for $r_0 = 20$ meters and remains of same order when r_0 varies from 5 meters to 20 meters. Due to random nucleation of the bubble, the off-diagonal component of components of the moment of inertia, as well as the quadrupole moment become nonzero. The ratio of both to the initial moment of inertia are found to be of same order, $\frac{Q}{I_0} \simeq \frac{I_{xy}}{I_0} \simeq 10^{-11} - 10^{-10}$.

B. Density Fluctuation From Topological Defects

The formation of topological defects routinely occurs in symmetry-breaking transitions and has been extensively discussed in the literature, from the early Universe to condensed matter systems. Depending on the relevant energy scales these defects can be a source of large density fluctuations. The underlying dominant mechanism for their formation in a phase transition is the so-called Kibble mechanism [76, 77] which predicts a defect density proportional to the number density of correlation domains, with proportionality constant determined using universal arguments depending only on the specific symmetry breaking pattern and dimensionality of space under consideration. Thus, the random network of defects arising in any phase transition and resulting defect distribution can be determined entirely using the symmetry-breaking pattern. For example, a random network of vortices arises from superfluid transition. A network of domain walls and global strings arises from the spontaneous breaking of $Z(3)$ center symmetry for confinement–deconfinement QCD transition [78]. Some QCD transitions (e.g. the color flavor locked (CFL) phase, expected to arise at very large values of baryonic chemical potential) may give rise to only global strings, with $SU(3)_c \times SU(3)_L \times SU(3)_R \times U(1)_B$ symmetry broken down to the diagonal subgroup $SU(3)_{c+L+R} \times Z_2$ [5]. The evolution of such a defect network shows universal characteristics. Starting with initial defect densities (basically determined using correlation length and topological probability calculations), the later evolution of string defects and domain wall defects shows scaling behavior. This has important implications for predictions

of changes in the moment of inertia (hence glitches/anti-glitches), quadrupole moment, and subsequent relaxation to the original state of rotation in a reasonably model-independent way. An important aspect of topological defect sourced density fluctuations relates to the manner in which density fluctuations evolve in time. Eventually density fluctuations decay away, leaving uniform new phase (in the core region undergoing phase transition). But the manner of this decay, and the time duration, depend crucially on the specific nature of the defect, and hence on the symmetry breaking pattern. For example, while bubble-generated density fluctuations decay away quickly in the time scale of coalescence of bubbles, the domain wall network and the string network coarsen on much larger time scales (with specific scaling exponents) which are characteristic of specific type of defect. Thus the precise measurement of the pulsar spinning rate and modification of pulse profile, and its time evolution, can also provide important information about the specific transition occurring inside the neutron star.

1. Lattice simulation of string network

Due to topological nature of these defects, generic features of the defect network can be determined using simple lattice picture with lattice size representing the correlation length. An estimate of the change in MI due to string and wall formation can be made by producing a network of defects inside the core of the pulsar by modelling the correlation domain formation in a cubic lattice, with lattice spacing ξ representing the correlation length [79]. To model $U(1)$ global string formation each lattice site is associated with an angle θ (randomly varying between 0 and 2π), or two discrete values 0, 1 while modelling Z_2 domain wall formation. (Z_2 domain wall is considered instead of Z_3 walls of QCD just for simplicity). For string case geodesic rule [76, 77, 79] is used to determine the winding of θ on each face of the cube.

Starting with correlation length of order of fm to simulate the network of order few hundreds meter is numerically not possible. So the estimates were made in [19, 20] by considering spherical star of size R and a spherical core of radius $R_c = \frac{0.3}{10}R$. Then, considering $\xi = 10fm$, R_c is increased from 5ξ to 400ξ , and it was found that $\frac{\Delta I}{I_i} \simeq$ appears to stabilize at $10^{-13} - 10^{-14}$. Using this numerical results, it was suggested that the same fractional change in the MI may also be possible for realistic value of $R = 10 \text{ km}$, especially when one accounts for statistical fluctuations in the core. For the case of domain wall formation, one finds fractional change in the off-diagonal components of MI (as well as quadrupole moments) to be larger by a factor of 40. For the case of superfluid transition, a rapid superfluid transition can take place due to transient heating, and subsequent cooling of star. This may occur either due to another transition releasing latent heat, or due to accretion, etc.. Taking vortex

energy per unit length to be $100\text{MeV}/\text{fm}$ and correlation length for vortex formation of order 10fm ([13, 75]) it is found that the superfluid vortices induced transient fractional change in MI is of order 10^{-10} (compared to net fractional change in MI of order 10^{-5} as discussed in Section VIA). Also it was found that the ratios of the quadrupole moment and off-diagonal components of MI to the net MI of the pulsar are of order 10^{-10} .

2. field theory simulation of strings and domain walls

The technique proposed in [19, 20] has potential of using detailed observations of pulse modification to learn about precise nature of phase transition occurring inside the pulsar. For this, one would need to know specific nature of density fluctuations for different cases and their precise time evolution. As the relevant cases here refer to quantum field theory phase transitions, one has to resort to field theory simulations to get such details. Unfortunately, with typical length scales of such QFT phase transitions being microscopic (e.g. of order fm for QCD transition), one can only hope to do these simulations in very small spatial regions. (This is different from the case of bubble nucleation where generic arguments of strong supercooling were invoked to determine density fluctuations over macroscopic regions even for QCD transition. even for lattice modelling of defect networks as discussed above, one could consider relatively large lattice sizes.)

This was achieved in [19, 20] by studying string and wall formation in a field theory simulation for confinement-deconfinement (C-D) QCD transition using effective field theory Polyakov loop model. The expectation value of the Polyakov loop, $l(x)$, is the order parameter for the C-D transition [80, 81]. $l(x)$ vanishes in the confined phase and is non-zero in the deconfined phase where $Z(3)$ center symmetry (for the $SU(3)$ color group) is spontaneously broken as $l(x)$ transforms non-trivially under $Z(3)$. This gives rise to three different vacua for different value of $l(x)$ in QGP phase, leads to topological domain wall defects (which interpolate between different $Z(3)$ vacua) [82], and also string defects (QGP strings) forming at the junction of these $Z(3)$ walls [78, 83, 84]. (Note, we have used the notations $Z(3)$ and Z_3 interchangeably.) Defect formation is studied using field theory simulation of the evolution of $l(x)$ from an initial value of zero (appropriate for the confining phase) as the system is assumed to undergo a rapid transition (quench) to the deconfined phase (as in [85]). Use of quench is not an important point here as the formation of defects only requires formation of uncorrelated domains, and the size of the domains in this model has to be treated as a parameter as it is not possible to cover length scales of km (for star) to fm (QCD scale). Hence these simulations are necessarily restricted to system sizes of tens of fm only. The physical size of the lattice is taken as $(7.5\text{fm})^3$ and $(15\text{fm})^3$. Another possible phase transition is to the so called color flavor locked (CFL) phase

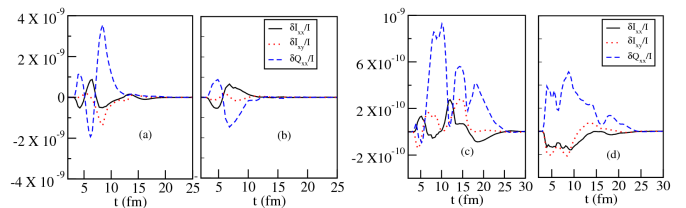


FIG. 6. Time evolution of fractional changes in the moment of inertia as well as the quadrupole moment during the process of phase transition. (a,b), and (c,d) correspond to lattice sizes $(7.5\text{fm})^3$ and $(15\text{fm})^3$ respectively. Plots in (a) and (c) correspond to the confinement-deconfinement phase transition which results in the production of $Z(3)$ walls and associated strings, while plots in (b) and (d) correspond to the transition where only string defects form which will be the case for the CFL phase. (Fig. taken from [19].)

inside the core of a pulsar where the QCD symmetry for three flavors (for very large baryon chemical potential such mass differences between these quarks become unimportant), $SU(3)_c \times SU(3)_L \times SU(3)_R \times U(1)_B$ is broken down to the diagonal subgroup $SU(3)_{c+L+R} \times Z_2$ [5, 86]. This transition will give rise to global strings. To roughly estimate resulting change in MI, a simplified case is considered by removing the cubic term from effective potential. This modification in the potential gives rise to string defects only without any domain walls, as appropriate for the transition from, say, QGP phase to the CFL phase, while ensuring that one has the correct energy scale for these string defects.

Fig. 6 shows how the induced fractional off-diagonal MI components and ratio of quadrupole moment to MI change in time. Even though the exact values of these quantities remain to be determined for the truly macroscopic core sizes (as for the lattice simulation of defect network discussed above), it is clear that in principle, exact temporal profile of these quantities can be determined. Thus resulting pulse modifications can be predicted in complete detail, in principle. One important, completely robust feature of these results is that density fluctuation induced contributions to even the diagonal components of the MI tensor can be positive as well as negative (with equal probability). These changes in diagonal components can then account for glitches as well as anti-glitches in the same unified framework. For this it is important to note that density fluctuations arise during phase transition to a new phase which by itself leads to change in the spin rate. Thus, when density fluctuations die away, the original spin rate is only partially restored (depending on the density difference between the two phases). This is precisely the qualitative behavior observed for glitches.

VII. PULSE MODIFICATION FOR RANDOM DENSITY FLUCTUATIONS

As we discussed above, in principle, a detailed analysis of perturbed pulses should be able to reveal a wealth of information about underlying density fluctuations occurring inside a pulsar. The order of phase transition, the symmetry breaking pattern, the time scale of phase transition, etc. will leave distinctive characteristic perturbations on the pulses. For this, one should consider specific source of density fluctuation, with well defined distribution of density fluctuations, and calculate in detail the resulting pulse modification. However, certain aspects of generic density fluctuations, in particular those resulting from any phase transition, will have qualitative implications for pulse modifications. Such density fluctuations will be statistical in nature, and will lead to random contributions to the components of the MI tensor. A general study of such fluctuations was carried out by some of us in [21] where the density fluctuations were modeled in terms of Gaussian distributed random components of MI tensor added to the unperturbed diagonal MI tensor of the neutron star. With the form of perturbed MI tensor prescribed, the resulting effects on pulse timings as well as specific nature of pulse modulations was then calculated. An important finding in [21] was that even for very tiny density fluctuations, with resulting changes in pulsar timings being extremely small, pulse profile modification were found to become relatively large due to modulations resulting from wobbling of NS. Main reason for this was that while pulse timing changes remain proportional to typical density fluctuation magnitude ϵ , the pulse profile modification were found to be proportional to ϵ/η^2 where η is the NS deformation parameter. (η is typically very small $\sim 10^{-8} - 10^{-4}$. This observation will play an important role in later discussion when we discuss possible detection of external GWs using NS deformations.) We first discuss this case of random MI components from [21]. Subsequently, we will also briefly mention how this technique can be applied to cases where modified MI tensor is precisely known, for example, the case of specific density fluctuations occurring in neutron stars during collision with an asteroid.

Basic physics of calculations in [21] is to consider a reasonably symmetric initial configuration of neutron star with homogeneous density, and then incorporate effects of random density fluctuations on its rotational dynamics. The shape of the unperturbed pulsar was taken to be an oblate spheroid, rotating about the z -axis with angular frequency ω and angular momentum $L_z = L$ ($L_x = L_y = 0$). The principal moment of inertia components were taken as $I_{11}^0 \equiv I_1^0 = I_{22}^0 \equiv I_2^0$ and $I_{33}^0 \equiv I_3^0 = I_0$ with $I_0 > I_1^0, I_2^0$. The oblateness is parameterized through $\eta = (I_0 - I_1^0)/I_0$, the value of which depends on the neutron star's mass, the rigidity of the crust and magnetic field etc. Theoretical studies by [87, 88] put the upper bound of η as $\simeq 10^{-6}$, whereas work of [89] puts the upper bound limit as 10^{-4} . Observational

studies put the upper bound close to $10^{-5} - 10^{-4}$ [90] with some pulsars having $\eta \sim 10^{-2} - 10^{-3}$ [91].

Immediately after a phase transition (at $t = 0$), density fluctuation will alter the MI tensor of the pulsar. The S_0 frame in Fig. 7 shows the set of principal axes immediately after the phase transition. The subsequent dynamics of the perturbed pulsar are governed by the set of Euler equations, [92, 93]

$$I_1 \dot{\omega}_1 - (I_2 - I_3) \omega_2 \omega_3 = 0 \quad (8)$$

$$I_2 \dot{\omega}_2 - (I_3 - I_1) \omega_1 \omega_3 = 0 \quad (9)$$

$$I_3 \dot{\omega}_3 - (I_1 - I_2) \omega_1 \omega_2 = 0. \quad (10)$$

Where I_i ($i = 1, 2, 3$) denotes the principal MI tensor components relative to the body fixed frame (S' in Fig. 7) and $\omega_1(t), \omega_2(t)$, and $\omega_3(t)$ are the angular frequencies of the star with respect to space fixed frame (which momentarily coincides with S'). As ω_1 , and ω_2 are expected to be very small compared to $\omega_3 \simeq \omega$, one can write the equation of motion for ω_1 as

$$\ddot{\omega}_1 + \Omega^2 \omega_1 = 0, \quad (11)$$

$$\text{where, } \Omega = \omega_3 \left[\frac{(I_3 - I_1)(I_3 - I_2)}{(I_1 I_2)} \right]^{1/2}. \quad (12)$$

Here, Ω is the precession frequency due to the perturbation. We consider the situation when perturbations are tiny in comparison to the oblateness parameter ($\epsilon \ll \eta$), hence the condition that $I_3 > I_1, I_2$ is still valid (as we will see below). The solution of the above equation is then given by

$$\omega_1(t) = A \cos(\Omega t) + B \sin(\Omega t). \quad (13)$$

A and B are two arbitrary constants determined from the initial conditions. Similarly using Eq. (13) and Eq. (9), one obtains the time evolution of ω_2

$$\omega_2(t) = k[A \sin(\Omega t) - B \cos(\Omega t)]. \quad (14)$$

Where the factor k is given by

$$k = \left[\frac{I_1(I_3 - I_1)}{(I_2(I_3 - I_2))} \right]^{1/2}. \quad (15)$$

The time $t = 0$ is assumed to be the onset of the pulsar's precession immediately after the completion of phase transition. Denoting the respective angular velocities at $t = 0$ by ω_1^0 and ω_2^0 respectively, Eqs. (13) and (14) can be rewritten as

$$\omega_1(t) = \omega_1^0 \cos(\Omega t) - \frac{\omega_2^0}{k} \sin(\Omega t) \quad (16)$$

$$\omega_2(t) = k \omega_1^0 \sin(\Omega t) + \omega_2^0 \cos(\Omega t). \quad (17)$$

Here, the arbitrary constants ω_1^0 and ω_2^0 can be fixed by initial conditions.

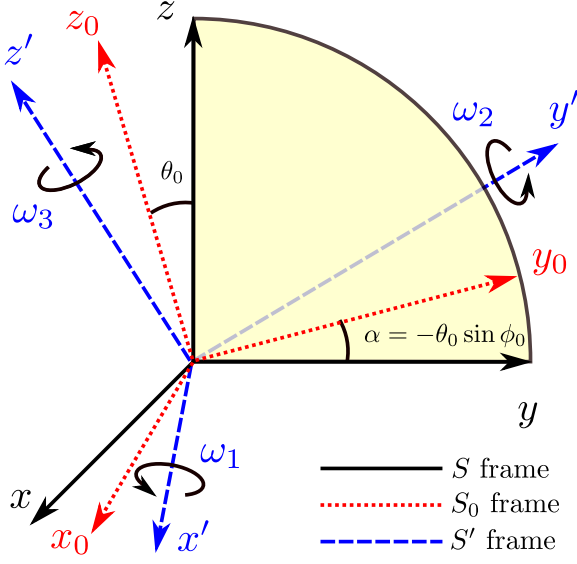


FIG. 7. An oblate shape unperturbed pulsar is initially (i.e. before any phase transition) rotating about the z -axis relative to a space-fixed frame S (solid black lines). The red dotted lines show the principal axes (x_0, y_0, z_0) of S_0 frame immediately after the phase transition (at $t = 0$). The body-fixed S' -frame at any arbitrary time $t > 0$ is shown with blue dashed lines (taken from [21]).

A. Initial conditions and analytical estimates of various parameters

Immediately after the phase transition, the orientation of the principal axes (S_0 frame) is shown in Fig. 7. The standard polar angle and the azimuthal angle of z_0 axis with respect to the S frame are denoted by θ_0 and ϕ_0 . These angles are obtained by diagonalizing the perturbed moment of inertia tensor and finding the eigenvalues and the corresponding set of eigenvectors (see [21] for details). In the absence of external torque, the angular momentum of the pulsar must be conserved. Thus, after the phase transition, the components of the angular momentum along x_0, y_0 , and z_0 are given by

$$L_{x_0}(t=0) = I_1 \omega_1^0 = -L \theta_0 \cos \phi_0 \quad (18)$$

$$L_{y_0}(t=0) = I_2 \omega_2^0 = -L \theta_0 \sin \phi_0 \quad (19)$$

$$L_{z_0}(t=0) = I_3 \omega_3^0 = L. \quad (20)$$

Because ω_3 is approximately constant and the angle θ_0 is small for tiny density fluctuations, one can use the approximation $L/I_1 \simeq L/I_3 \simeq \omega$. The above set of equations can be used now to express Eqs. (13) and (14) in terms of θ_0 and ϕ_0 . Since the phase transition fluctuations are small, the perturbed MI tensor can be written

as

$$I_{1,2} = I_0(1 - \eta + \epsilon_{1,2}), \quad (21)$$

$$\text{and } I_3 = I_0(1 + \epsilon_3), \quad (22)$$

with $\mathcal{O}(\epsilon_i) \simeq \mathcal{O}(\epsilon)$ for $i = 1, 2, 3$. Therefore the precession frequency (Eq. (12)) can be written as

$$\Omega \simeq \left(\frac{\eta + \epsilon}{1 - \eta + \epsilon} \right) \omega \simeq \eta \omega. \quad (23)$$

Here it is assumed that $\epsilon, \eta \ll 1$ and $\epsilon \ll \eta$. The initial angle θ_0 is obtained by diagonalizing the perturbed MI tensor I_{ij} . For an order of magnitude estimate, the perturbation $\epsilon_{ij} \equiv \delta I_{ij}/I_0$ can be taken as $\epsilon_{ij} = \epsilon/I_0$. This results in

$$\cos \theta_0 = \left(1 + 2 \left(\frac{\epsilon I_0}{I_3 - I_1 - \epsilon I_0} \right)^2 \right)^{-1/2}. \quad (24)$$

Assuming $\epsilon \ll \eta$, one gets $\theta_0 \simeq \sqrt{2} \left(\frac{\epsilon}{\eta} \right)$. On similar argument, one obtains the factor $k = 1 + \epsilon/2\eta$. Thus, the Eq.(16) and Eq.(17) can be expressed as

$$\omega_1(t) = -\omega \theta_0 \left[\cos(\Omega t + \phi_0) + \frac{\epsilon}{2\eta} \sin \phi_0 \sin(\Omega t) \right] \quad (25)$$

$$\omega_2(t) = -\omega \theta_0 \left[\sin(\Omega t + \phi_0) + \frac{\epsilon}{2\eta} \cos \phi_0 \sin(\Omega t) \right]. \quad (26)$$

The corresponding rotational angles $\theta_1(t)$ and $\theta_2(t)$ can also be re-expressed as

$$\theta_1(t) = -\frac{\omega \theta_0}{\Omega} \left[\sin(\Omega t + \phi_0) - \frac{\epsilon}{2\eta} \sin \phi_0 \cos(\Omega t) \right] \quad (27)$$

$$\theta_2(t) = \frac{\omega \theta_0}{\Omega} \left[\cos(\Omega t + \phi_0) + \frac{\epsilon}{2\eta} \cos \phi_0 \cos(\Omega t) \right]. \quad (28)$$

Putting the values of Ω and θ_0 , the amplitude ω_m (From Eqs. (25) and (26)), and θ_m (From Eqs. (27) and (28)) are determined as

$$\omega_m = \omega \theta_0 \simeq \sqrt{2} \left(\frac{\epsilon}{\eta} \right) \omega, \quad (29)$$

$$\theta_m = \left(\frac{\omega}{\Omega} \right) \theta_0 \simeq \sqrt{2} \left(\frac{\epsilon}{\eta^2} \right). \quad (30)$$

Thus for $\eta = 10^{-3}$, the oscillation amplitude θ_m is of order $10^6 \epsilon \simeq 1^\circ$ for $\epsilon = 10^{-8}$. It was shown in ref. [21] that the above analytical estimates approximately match the results obtained from the simulation.

B. Numerical Results

Here we briefly review the simulation results of Ref. [21]. There, two sets of values $(\eta, \epsilon) = (10^{-2}, 10^{-5})$ and

($10^{-3}, 10^{-8}$) were chosen to observe the impact of perturbation on pulse modulations (See Table 1 in [21] for the values of other parameters). Note that Eqs. (25) and (26) can be approximately written as $\omega_{1,2} \sim \omega_m \cos(\Omega t)$. Since $\Omega \sim \eta\omega$ (Eq. (23)), the time period $T_\Omega = T_\omega/\eta$. Thus $T_\Omega = 0.1$ for $\eta = 10^{-2}$ and 1 sec for $\eta = 10^{-3}$. This matches the numerical simulation results in Ref. [21]. The results are shown in Figs. 8, and 9.

Other than the above (first) modulation, another (second) modulation is also expected since ω_1 and ω_2 also oscillates about the x and y axis, respectively. From the frequency oscillation amplitude $\omega_m \sim (\epsilon/\eta)\omega = (2\pi\epsilon/\eta)1000$ /sec., the second modulation time scale can be approximately determined as $T_m \simeq 10^{-3} (\eta/\epsilon)$ sec. Thus, the time scale T_m varies from a few seconds [for $(\eta, \epsilon) = (10^{-2}, 10^{-5})$] to a few hundred seconds [for $(\eta, \epsilon) = (10^{-3}, 10^{-8})$]. The figures 8, and 9 indeed show that there is a second modulation, though the numerical results show time scale is larger compared to the analytical estimate T_m . (For clarity, in Fig. 9, only the top part of the pulses is shown compared to Fig. 8.) Of course, considering the complexity of the rigid body dynamics, and the order of magnitude estimates used, one can expect uncertainty in the analytical estimates of the concerned quantities.

An important feature of these results can be termed as *the memory effect*. This relates to the fact that, even after the density fluctuations fade away leading to vanishing off-diagonal components, thereby restoring the original rotation axes, and hence the original pulse profile, there will in general be a net shift of the angular position of the pulse. (This is apart from the effect of any possible net change in the spin rate. So, if net spin rate change remains unobservable, this net shift of the angular position may still be observable as it originates from the transient pulse modification from intermediate stage of wobbling of star.) Therefore, a net, residual shift of the angular position of the pulse could signal a missed phase transition.

C. Pulse modification due to asteroid impact on neutron star

Impact of asteroids, comets etc. on astrophysical bodies frequently occur and with intense gravity of neutron stars, such impacts have dramatic effects. For example, it has been proposed that certain specific gamma ray burst event may have origin in the impact of a solid body (comet or asteroid) with mass of order 10^{18} g colliding with NS surface [94]. The tidal distortion of the body during last stages of impact, with intense magnetic field of neutron star leads to strong compression between magnetic longitudes. The interaction of this with NS surface material, with exploding material falling back at magnetic conjugate points was studied in detail in [94] and it was proposed that it could explain specific gamma ray burst events. In view of discussions in previous sec-

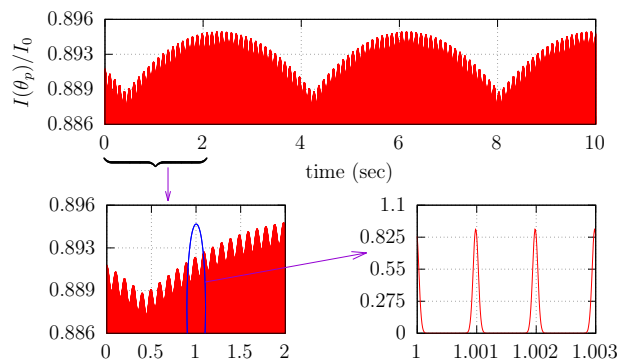


FIG. 8. The figure shows the time evolution of the pulse profile $I(\theta_p)/I_0$ of a millisecond pulsar for $(\eta, \epsilon) = (10^{-2}, 10^{-5})$. The top plot shows the two different modulations at different time scales. Bottom-left shows the same plot with better resolution. Bottom-right shows a few pulses for a typical millisecond pulsar. The figures are taken from [21].

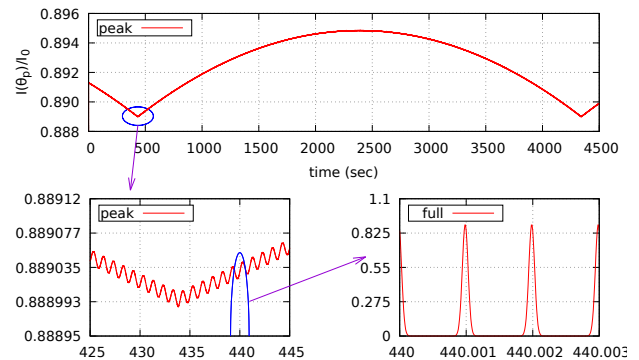


FIG. 9. (taken from [21]) Same plot as Fig. 8, however for $(\eta, \epsilon) = (10^{-3}, 10^{-8})$. An apparent ‘kink’ at the top figure appears just below 500 s smoothed out with improved resolution (bottom-left). For clarity, here only the top part of the pulses is shown compared to Fig. 8.

tions, it becomes natural to expect that such a collision occurring on the surface of a pulsar should lead to perturbation in the MI tensor of the pulsar, and hence should leave imprints on the pulses. This interesting possibility is explored in [95]. Special feature of this case is that, in this case, one can determine exact modification of the MI tensor of the pulsar. This is done by following detailed impact dynamics of the body on the NS surface as calculated in [94]. With the perturbed MI tensor known, it is then straightforward to apply the technique discussed above, and determine the detailed nature of perturbed pulses. One important unknown in this case is the NS deformation parameter η which determines the pulse modulations (as discussed above). As resulting change in MI tensor will have very small magnitude in this case (with ϵ of order 10^{-15} for a 10^{18} g body impacting on a solar mass NS), observation of pulse modulations will only be

possible for NS with very small values of η . Still, this suggests an interesting technique to probe impact of bodies on pulsar surfaces by observing pulse modifications. In particular, for any proposed explanations on gamma ray bursts etc., one will expect an accompanying observation of pulse modification (depending on value of η).

VIII. GRAVITATIONAL WAVES DUE TO PHASE TRANSITION INDUCED DENSITY FLUCTUATIONS

Here we discuss how phase transitions occurring inside neutron stars may provide a new *high frequency* source of gravitational waves through density fluctuation induced rapidly changing quadrupole moment of the star.

Neutron stars are considered to be one of the most sought after sources of gravitational waves. As the emission mechanism from such a source is governed by its internal structure, searches for gravitational waves from such a source can provide valuable information. For example, through a series of works, Thorne et al. [96–99] developed a non-radial pulsation theory for a general relativistic static neutron star model. The author suggested that various mechanisms can excite quasinormal modes of the parent neutron star and may result in gravitational wave emission. The mechanisms capable of exciting quasinormal modes include flaring activity, the formation of hypermassive neutron stars following the coalescence of binary neutron stars etc. The mechanism associated with the timing glitch can excite quasinormal modes in the parent pulsar also. With this motivation, the searches for the emission of GWs from isolated pulsars began even before the first ever direct detection of GWs from the binary black hole merger. In this context, an attempt for GW search associated with the timing glitch in the Vela pulsar in August 2006 [47] is worth mentioning. Although the above search produced no detectable GWs, with improving sensitivity of the detectors, continuous attempts in this direction are believed to yield fruitful results soon.

In the literature, there are a few other theoretical studies where the authors [44–46, 87, 100] have explored the feasibility of emission of gravitational waves from isolated pulsars (see the review [101] for more details). These studies considered various reasons for GW emissions. These include the existence of deformity of neutron stars in the form of crustal mountains on the surface [44], or permanent triaxiality [45] of the star. This mechanism, as mentioned above, produces monochromatic GWs, the frequency of which is determined by the spin frequency of the star. There was also a suggestion that crustquake (see V) may have a role in generating GWs [46, 102]. In reference [102], the authors considered the crustquake as a trigger which can excite various oscillatory modes of the pulsar [102], causing emission of GWs. The role of crustquake as a possible source of GWs was also suggested in [46], where the authors noticed that the sudden

change of the oblateness corresponded to a change of the quadrupole moment within a very small time scale and crustquake could indeed cause the bursts of GWs [46]. In the context of bursts of GWs from an isolated pulsar, we will discuss the case discussed in [19] where density fluctuations induced during phase transitions were discussed. These density fluctuations were found to perturb the entire MI tensor of the neutron star. Along with that, it also necessarily produced non-zero quadrupole moment. With a very short time scale associated with the phase transition, e.g. for a QCD phase transition, in [19], it was suggested the rapidly evolving quadrupole moment can provide a new source of gravitational waves.

In [19], the authors have discussed how density perturbations due to bubble nucleation or formation of topological defects during phase transitions change the moment of inertia (MI) tensor of the star, in general with the addition of off diagonal components in the MI tensor. In other words, the rotation axis of the star no longer remains aligned with one of its principal axes. As the shape of the star diverges from sphericity during phase transition, it develops a quadrupole moment Q also. The quadrupole moment tensor Q_{ij} ($i, j = 1, 2, 3$) varies rapidly during phase transition, thereby giving rise to quadrupolar gravitational radiation. In the weak field limit, the power emitted by the star through gravitational radiation is given by [103]

$$\begin{aligned} \frac{dE}{dt} &= -\frac{32G}{5c^5}(\Delta Q)^2\omega^6 \\ &\approx -(10^{33} J/s) \left(\frac{\Delta Q/I_0}{10^{-6}}\right)^2 \left(\frac{10^{-3} s}{\Delta t}\right)^6. \end{aligned} \quad (31)$$

Here, we use ΔQ to represent generic value of ΔQ_{ij} which is the change in the ij^{th} component of the quadrupole moment tensor during a time interval Δt and I_0 is the initial moment of inertia of the spherical NS. (The above expressions were derived in [103] for a periodically varying quadrupole moment with angular frequency ω . As our aim here is only to provide the possibility of phase transition induced density fluctuations being a new source of GWs, we use these expressions with the typical time scale of the phase transition as playing the role of the period associated with ω . The important factors to be noted above are $(\Delta Q)^2$ and ω^6 leading to $(\Delta t)^{-6}$ dependence for the GW power with Δt being the time scale of the phase transition.) According to [19], $\frac{\Delta Q_{ij}}{I_0}$ lies within the range $10^{-11} - 10^{-10}$ for phase transition through bubble nucleation and within the range $10^{-14} - 10^{-10}$ when inhomogeneities in density of the star arise due to formation of topological defects (see for example Table 1 of [19]). Though this value is much lower than the typical value of 10^{-6} used for deformed neutron stars, the fact that the change in Q occurs over a time scale of microseconds (as a conservative estimate) makes the power radiated by gravitational waves in this situation significant. An estimate of the strain amplitude h arising from a pulsar

at a distance r from the field point is given by

$$h = \frac{4\pi^2 G \Delta Q f^2}{c^4 r} \approx 10^{-24} \left(\frac{\Delta Q / I_0}{10^{-6}} \right)^2 \left(\frac{10^{-3} \text{s}}{\Delta t} \right)^6 \frac{1 \text{kpc}}{r}. \quad (32)$$

Taking $\frac{\Delta Q}{I_0} \approx 10^{-10}$, $\Delta t \approx 10^{-6} - 10^{-5}$ s, and $r = 1 \text{kpc}$, they get $h \approx 10^{-24} - 10^{-22}$. In reality, Δt could be smaller, thereby enhancing h and dE/dt . Note that as the gravitational wave emission is extremely short lived, net energy lost by the star is negligible compared to its mass.

In conclusion, transient changes in MI of a pulsar due to phase transition induced density perturbations give rise to non-vanishing rapidly varying quadrupole moment and hence quadrupolar gravitational radiation. In general, the MI tensor in this case gets off diagonal contributions that cause wobbling of the pulsar and consequent modification of the peak pulse intensity. This is a special feature of the model of [19]. Through observation of modulation of peak pulse intensity and gravitational waves, it is possible to identify the specific nature of phase transition occurring within the core of the star.

IX. PULSAR AS A WEBER DETECTOR OF GRAVITATIONAL WAVES

So far we discussed the effects of internal dynamics of neutron star leading to density fluctuations and changes in the nature of pulses from the pulsar. In this section, and next, we will discuss the effects of an external gravitational wave on the neutron star configuration. It is natural to be sceptic, as expected deformations in NS will be extremely tiny. However, at the same time we also recall the impressive accuracy of pulsar timing observations, better than 1 part in 10^{15} . Further, as discussed above in Section VII, possible changes in the pulse profile from induced wobbling of pulsar may be large, even if pulse timing changes remain very small. We will put forward arguments here that pulsars can effectively act as *remotely stationed* resonant Weber detectors whose GW perturbed signals may be observable on earth. Such a possibility is worth exploring, even if it requires challenging observations. Many gravitational wave detectors (like LIGO/Virgo) are being set up around the globe, in order to be able to detect gravitational waves with good localization of the source in the sky. This will be complemented by future space-based detectors for the search for gravitational wave sources with very wide range of wavelengths and strengths. However, even all these near earth detectors will be limited in their scope as most of the powerful gravitational wave sources occur very far and also, triangulating the location of the sources will also be limited. Clearly, if one could have a family of detectors placed far away in space, so that their signals

could be monitored on earth, that will immensely boost our ability for detecting and identifying GW sources.

The discussion in this section is taken primarily from ref.[22]. Basic physics proposed here is, to put it simply, taking the entire neutron star as a *resonant Weber detector*. While for the conventional Weber detectors [104–107], GW induced deformations are detected and converted into electrical signals, for neutron stars (pulsars), deformations induced by external GWs will be imprinted on the detailed nature of pulses which can be monitored on earth. As for the conventional Weber detector, resonance will play a crucial role for pulsar Weber detectors also which will lead to amplitude enhancement, and more importantly, the *ringing effect* [107] which will allow folding of a large number of pulses to tremendously improve the signal to noise ratio.

It is important to make a distinction between the proposal here for using pulsar itself as a Weber detector, and the conventional technique of pulsar timing array (PTA) for GW detection [108]. For PTA, one monitors the pulse arrival times from a network of pulsars, and looks for gradual changes due to passage of very low frequency gravitational waves in the intervening region. By its very nature, PTA technique is limited to extremely low frequency sources with frequencies of order 10^{-6} Hz or less. Such GWs are expected to arise from supermassive black hole mergers or exotic objects such as cosmic strings. In contrast, for the technique discussed here, a single pulsar acts as a GW detector. In principle, even a single pulsar Weber detector can give some information about the GW source direction through changes in its spin rate and pulse profile. In the context of the proposal made here, we note that it was proposed long ago [109] that with an array of seismometers, the whole earth may be used as gravitational wave detector for low frequency GWs. Proposals have also been made that gravitational waves may be detected due to their effects on nearby stars, in particular on the solar acoustic modes (helioseismology and astro-seismology) [110–112]. There is some similarity in spirit of these proposals with the pulsar Weber detector proposed here. However, to our knowledge, detection of GW using its effects on pulse modifications of a pulsar [22], had not been discussed earlier.

Consider a monochromatic gravitational wave with wavelength λ from a far away GW source, reaching a neutron star. Passing of GW means periodic changes in the Riemann curvature tensor $R_{\mu\nu\lambda\rho}$ which will induce deformations of any body in its path. For a neutron star, one can calculate changes in its quadrupole moment Q_{ij} induced by a GW in the static limit (essentially, large wavelength limit for the GW compared to the neutron star size). It can be written in the following form [113]:

$$Q_{ij} = -\lambda_d E_{ij}. \quad (33)$$

Here, $E_{ij} = R_{i0j0}$ is the external tidal field. λ_d is called the tidal deformability,

$$\lambda_d = \frac{2}{3} k_2 \frac{R^5}{G}. \quad (34)$$

Here R denotes the equilibrium (undisturbed) radius of the neutron star and k_2 is called the second Love number. There have been theoretical estimates of this. For polytropic pressure-density relation $P = K\rho^{1+\frac{1}{n}}$, where K is a constant and n is the polytropic index, numerical results (for $0.5 \leq n \leq 1.0$, and $0.1 \leq (M/R) \leq 0.24$) can be fitted by the formula [113].

$$k_2 \simeq \frac{3}{2} \left(-0.41 + \frac{0.56}{n^{0.33}} \right) \left(\frac{M}{R} \right)^{-0.003} \quad (35)$$

Remarkably, the BNS merger event detected by LIGO/Virgo [18] has been used to put a direct observational constraint on the value of k_2 to lie within the range, $k_2 \simeq 0.05 - 0.15$, and we will be using values of k_2 within this allowed range.

For a GW travelling along z direction, the tidal field E_{ij} can be calculated for the two polarizations ('+', and 'x') polarizations) in the transverse traceless (TT) gauge. We consider the '+' polarization and denote the gravitational wave strain amplitude by h for this polarization. The resulting tidal field amplitude is given by [114],

$$E_{xx} = -E_{yy} = \frac{2\pi^2 hc^2}{\lambda^2}, \quad (36)$$

We take the neutron star to have a spherical shape and mass M . This tidal field of the gravitational wave will then induce a quadrupole moment tensor as given above in Eq.(33). Taking this deformation to be of an ellipsoidal shape, one can estimate the resulting change in the moment of inertia tensor of the neutron star.

$$\frac{\Delta I_{xx}}{I} = -\frac{\Delta I_{yy}}{I} \simeq \frac{k_2}{3} \frac{R^3 c^2}{GM\lambda^2} 20h \quad (37)$$

For sample values, $M = 1.0M_\odot$ and $R = 10$ km and λ for a gravitational wave with 1 kHz frequency (for GW from a typical astrophysical source, as detected by LIGO/Virgo).

$$\frac{\Delta I_{xx}}{I} \simeq 10^{-2} h. \quad (38)$$

Here we have used a sample value $k_2 = 0.1$ within the allowed value from BNS merger event [18]. This event had the GW source about 130 million light years away from earth, and had the peak strength of the signal $h \simeq 10^{-19}$. The advantage of the proposed pulsar Weber detector is that it could be anywhere in space. Most optimistically, one can even imagine that a pulsar was about 1 light years away from the BNS undergoing merger. (Such a possibility can be considered as most neutron stars and pulsars arise in globular clusters in our galaxy, so one could imagine it to be also true for other galaxies, i.e. for this particular BNS event, though extragalactic pulsar observations are not very frequent). The value of h at the location of that pulsar will be about $h \simeq 10^{-11}$. As the spin rate change for the pulsar is directly related to change in its MI, change in the spin rate

of the pulsar will be

$$\frac{\Delta\nu}{\nu} = \frac{\Delta I}{I} \simeq 10^{-13}. \quad (39)$$

where ΔI represent the change in the relevant component of MI. Given the extreme levels of accuracy of measurements of pulsar signals, this magnitude of spin rate change is well within observations. It is important to note that for a generic direction of propagation of the GW, the MI tensor will develop non-zero off-diagonal components also. This will induce wobbling of the pulsar leading to the modulation of the pulse intensity profile. Exactly this type of modulation was discussed above in Section VII. One important result from that section is that even for very tiny changes in the spin rate due to changes in the diagonal components of MI tensor, induced wobbling (and hence changes in the pulse profile) may be much larger, especially for neutron stars with small deformation parameter η . Thus profile changes may become more important as a signal of GW passing through a pulsar. However, in this section we will keep focusing on the spin rate change, as profile change discussion is much more involved. Discussion of Section VII can be straightforwardly applied to the present case of GW induced changes in the MI tensor.

A crucial requirement for the Weber detector is that it needs to work at resonance. The resulting increase in amplitude is not too large as GW signals are short pulses, limiting resonant enhancement of the amplitude. However, at resonance, the solid detector exhibits the so called *ringing effect*. Ringing effect refers to continued vibration of the detector in the resonant mode for a long time even after complete passing of the GW pulse through the detector. This happens because at resonance energy absorption from the wave is highly efficient. That energy has to be dissipated in sound and heat, until then the detector will keep vibrating. For example, for a GW pulse of duration a few ms, at resonance, the vibrations of the Weber bar can continue for time of order 10 min [106, 107]. With the particular template for the pulse, a large number of pulses, getting repeated during this ringing, can be folded. This leads to tremendous increase in the signal to noise ratio. In the same way, for the pulsar Weber detector working at resonance, one would expect the pulsar to continue *ringing* for a long time after the passing of the GW. This should allow folding of many pulses to separate this *ringing* signal. In fact, this is the standard way in which a large number of regular pulses from the pulsar are folded, leading to impressive accuracy of pulse timings. The difference is that regular pulses from the pulsar are periodic, and hardly change in relevant time scales (apart from occasional glitches), so pulse folding is standard. The ringing of pulsar Weber detector shows that even for a short GW pulse, similar folding of large number of pulses may be possible.

There is a wide range of resonant frequencies for neutron stars with frequencies of few Hz all the way up to 20 kHz [115]. For specific modes, the resonant frequencies of

NS can be in the Range of 100 Hz to 1 kHz, which is precisely the range relevant for a typical BNS merger GW source, also for typical black hole mergers (with masses within tens of solar masses).

A. The quality factor Q for the neutron star matter

Effectiveness of Weber detector crucially depends on the quality factor Q of the detector material. Very high values of Q will lead to better enhancement in the vibration amplitude. More importantly, the energy dissipated per vibration cycle will be low, prolonging the ringing effect, thereby allowing folding of much larger number of pulses for better signal to noise ratio. It has been argued that various viscous effects may not be very important even on time scales of the orbital decay time [116]. Thus it is entirely possible that the quality factor Q for neutron star interior may be very large, possibly much larger than the material available on earth for conventional Weber detectors. Thus, one needs to know the Q factor for NS interior. This is a new challenge for QCD calculations, apart from the well known problem of determining the equation of state, and transport coefficients like shear viscosity, the quality factor Q for different phases of QCD (at least for the hadronic and the QGP phases) needs to be calculated. It is illuminating to quote here from the review article on *Detection of gravitational waves* [117]. In the section on the Antenna materials for the resonant-mass (Weber) detectors, it is stated,

"An ideal resonant bar would consist of a piece of nuclear matter, with high density and a velocity of sound comparable to the velocity of light! Since this is not available except in neutron stars, we must find a form of molecular matter which, to maximize coupling to gravitational waves, combines high velocity of sound v_s , and high density ρ . To reduce the thermal noise we require a low acoustic loss Q^{-1} ".

The arguments presented in this section propose that, going with the spirit of above quotation, we realize that neutron star material can possibly be available for use in a Weber detector, in fact by using the entire neutron star itself as a pulsar Weber detector.

X. RE-VISITING PAST GRAVITATIONAL WAVES VIA PULSARS AS WEBBER DETECTORS

An interesting outcome of the possibility of using pulsars as Webber gravitational wave detectors spread out in the cosmos is that they can be used to revisit past GW events, like collisions of black holes, neutron stars, supernova explosions etc., again and again. These past events are taken to be such that their signals have already passed through Earth. They might have been detected by LIGO/Virgo or their signals might have been missed. Supernovae within our galaxy whose existence have been de-

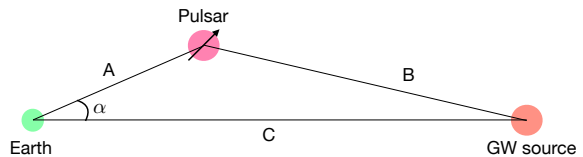


FIG. 10. Schematic diagram showing the relative positions of Earth, a distant GW source and a pulsar whose change in pulse profile and spin rate we can measure on Earth. (Fig. taken from [23].)

duced from astronomical data collected around the world fall within the latter category. This novel idea has been proposed in [23]. Figure 10 schematically represents the situation we are talking about. Gravitational waves from the source directly travel to Earth via path C but it also travels to a pulsar via path B, transiently inducing a quadrupole moment in the pulsar and changing its moment of inertia and hence its pulse frequency and profile. The modified pulses reach earth via path A. If $r_{A,B,C}$ are the distances along paths A, B, C respectively then the path length difference between the direct path C and the path A+B via a pulsar is,

$$\Delta r = (r_A + r_B) - r_C, \quad (40)$$

$$= r_A + (r_A^2 + r_C^2 - 2r_A r_C \cos \alpha)^{1/2} - r_C. \quad (41)$$

Thus, the indirect signal will be detected on Earth a time t_0 after the arrival of the direct signal, where

$$t_0 = \frac{\Delta r}{c}. \quad (42)$$

Angle α between the directions of the GW source and the pulsar is given by $\alpha = \cos^{-1}(\sin \theta_p \sin \theta_s + \cos \theta_p \cos \theta_s \cos(\phi_p - \phi_s))$, $\theta_{p,s}$ and $\phi_{p,s}$ being respectively the ‘Declination’ and ‘Right Ascension’ angles for the pulsar and GW source. Signals from pulsars that lie far away from Earth (i.e., r_A is relatively large) will arrive on Earth within a reasonably short interval after its direct detection only if α is small. For α close to zero, r_A doesn’t matter in eq. 41 and there is almost no time delay between the direct and indirect signals. (Thus, errors in pulsar distances do not affect the values of t_0 for small α .) In [23], the authors have presented an elaborate list of GW events, pulsars through whose signals the events may be revisited and the range of computed arrival times of the affected signals from the pulsars, accommodating for known errors wherever possible. Their data is available for past events whose earliest signal arrival dates lie within the next 100y after 1967 and also whose uncertainty in signal arrival dates is limited to within 100y. A notable example among many interesting cases is the earliest recorded supernova event SN185 that may become observable again via pulsars J0900-3144 and J1858-2216 between 2016-2049. A few other interesting cases are of supernovae SN1885 whose perturbed signal via pulsar B2310+42 is expected to reach Earth between

2022-2044 and SN1604 whose signal perturbed by pulsar J1813-1246 should reach between 1971-2052.

Thus, gravitational waves from events that have travelled through pulsars strewn in the sky can be observed again, not only once but multiple times, through the observation of perturbed pulses from these pulsars. Nature of modification of pulsar timing and pulse profile also depends on the relative directions of GW propagation and pulsar spin. So, even a single indirect pulsar-detector observation can be used to get information about source direction. However, an important question that may arise here is how would one determine whether the observed change in pulse profile/timing is indeed due to passage of gravitational waves and not some other phenomena like glitches or phase transition induced density perturbations in the core of the star. Of course, a careful analysis using detailed characteristics of the incoming GW signal (its profile and direction), the internal structure of the pulsar and the direction of observation on Earth is needed to confirm this. Yet, even without that, one can keep in mind the simple physical fact that any change in pulse profile due to passing gravitational waves will be temporary and the spin rate/pulse profile of the pulsar will be restored to the original value, unlike cases where glitches or density perturbations arising from phase transitions are the source of pulse modification. Except an important effect that there will in general be a net shift of the angular position of the pulse if there was any such transient GW event. This is exactly the same effect which was discussed in Section VII for any transient effect of phase transition induced density fluctuations. Thus, a net, residual shift of the angular position of the pulse could signal a missed phase transition or a missed GW event. To further distinguish between these two possibilities, we note that any phase transition will necessarily also lead to free energy changes which are permanent, thereby leading to permanent change in spin rate. In contrast, GW event is genuinely transient, without any permanent change of the NS structure. Thus the original spin rate will be completely restored.

XI. CONCLUSIONS AND FUTURE DIRECTIONS

Main focus of this brief review is on certain specific properties of pulsars, namely the extreme accuracy of observations of its pulses, and very sensitive dependence of the detailed nature of pulses, as observed on earth, on the internal structure of the pulsar. Probes of internal structure of neutron stars is of paramount importance in astrophysics. This has acquired special importance in view of the exciting detection of GWs from BNS merger events which have allowed direct probe of internal structure of the neutron star matter due to tidal deformation of the neutron stars during last stages of coalescence. Probing neutron star core structure is of great importance for understanding of the rich spectrum of

various exotic high baryon density phases of QCD. This part of the QCD phase diagram has so far eluded experimental observations in terrestrial experiments (relativistic heavy-ion collision experiments). Various estimates suggest that extreme baryon densities needed for several such phases may only become accessible inside neutron star cores. Detailed nature of pulses is extremely sensitive to any changes occurring in the rotational dynamics of the pulsar, hence to any changes occurring in the configuration of a pulsar. This makes pulsar observations as powerful probe of dynamical processes affecting pulsar structure. We have discussed how internal changes in pulsar due to various phase transitions occurring in the pulsar cores can leave detailed imprints on pulses. Changes in the equation of state directly affects the spin rate by affecting the diagonal components of the moment of inertia tensor. At the same time, phase transition induced random density fluctuations affect entire MI tensor, including its off-diagonal components. This induces wobbling of the pulsar, leading to modulation of pulses as observed on earth. It may thus be possible to infer about the detailed nature of specific phase transitions occurring in the pulsar core by detailed analysis of pulsar observations. Random density fluctuations during phase transitions also induce rapidly changing quadrupole moment of the neutron star, providing one more possible source of GW emission from neutron stars. A particular interesting possibility arises when one considers pulsars in the presence of external gravitational waves. While acknowledging the fact that GWs induce extremely tiny configurational changes in bodies, it has been proposed that extreme accuracy of pulsar observations may allow detection of such GWs, especially for GW frequencies in the resonant bands of the neutron star oscillations. This is precisely the physics of Weber detectors of gravitational waves. Pulsars, thus can act as remotely stationed resonant Weber detectors of GWs, with the signal of GW getting transmitted to earth in form of perturbations on the pulses. This also allows for very exciting possibility of detecting gravitational wave events of past, that is cases when GWs from distant sources passed through the earth in past. Same GWs also reach pulsars affecting its pulses. Those perturbed pulses are detected on earth much later, allowing us to re-visit past gravitational wave events.

Admittedly, the feasibility of this proposal of using pulsars as Weber detectors leaves many questions unanswered. Even with the ringing effect, which will allow for the folding of very large number of pulses, it is not very clear what level of GW strain amplitude will be observable by analysis of pulsar signals. The extreme accuracy of pulsar signals is also achieved only by folding huge number of pulses. One thing which will come to help here is that pulsar will probably be most perfect Weber detector possible, formed with extreme density QCD matter (recall the quotation in Section IX.A from ref. [117]). Further, ideal situation will be to have a BNS system where at least one partner is a pulsar. If one neutron

star emits GW, then the partner pulsar will carry large imprints of that signal to earth. Pulsar in this sense becomes permanent probe of any micro changes happening in the interior of the partner neutron star.

The most important aspect of pulsar being Weber detector will be that the detector has possibility of being very close to the GW source. It is clear, that the proposal will be most effective if extra-galactic pulsars can be monitored with great accuracy. Thus, importance of extra-galactic pulsar may be viewed in this term also, that, with these *pulsar Weber detectors* being out there,

chances of a powerful GW source being close-by may be significant, allowing us to see the imprints of those GWs on the signals of that pulsar.

ACKNOWLEDGMENT

This article is dedicated to the loving memory of Abira Sarkar. We also deeply acknowledge her immense support during the writing of this article.

-
- [1] L. P. Csernai, *Introduction to relativistic heavy ion collisions* (1994).
- [2] C. Y. Wong, *Introduction to high-energy heavy ion collisions* (1995), ISBN 978-981-02-0263-7.
- [3] U. Heinz and R. Snellings, *Ann. Rev. Nucl. Part. Sci.* **63**, 123 (2013), 1301.2826.
- [4] K. Rajagopal and F. Wilczek, *The Condensed matter physics of QCD* (2000), pp. 2061–2151, hep-ph/0011333.
- [5] M. G. Alford, A. Schmitt, K. Rajagopal, and T. Schäfer, *Rev. Mod. Phys.* **80**, 1455 (2008), 0709.4635.
- [6] K. Rajagopal, *Color Superconductivity* (Springer Netherlands, Dordrecht, 2002), pp. 475–522.
- [7] M. Alford, J. Bowers, and K. Rajagopal, *Journal of Physics G: Nuclear and Particle Physics* **27**, 541 (2001), URL <https://dx.doi.org/10.1088/0954-3899/27/3/335>.
- [8] E. Witten, *Phys. Rev. D* **30**, 272 (1984), URL <https://link.aps.org/doi/10.1103/PhysRevD.30.272>.
- [9] E. Farhi and R. L. Jaffe, *Phys. Rev. D* **30**, 2379 (1984).
- [10] C. Alcock, E. Farhi, and A. Olinto, *Astrophys. J.* **310**, 261 (1986).
- [11] J. E. Horvath, O. G. Benvenuto, and H. Vucetich, *Phys. Rev. D* **45**, 3865 (1992).
- [12] F. Weber, C. Kettner, and M. K. Weigel, in *Presented at the Symposium on Strangeness and Quark Matter* (1994), pp. 1–5.
- [13] C. H. Yang and J. W. Clark, *Nucl. Phys. A* **174**, 49 (1971).
- [14] M. Prakash, J. M. Lattimer, J. A. Pons, A. W. Steiner, and S. Reddy, *Lect. Notes Phys.* **578**, 364 (2001), astro-ph/0012136.
- [15] R. A. Hulse and J. H. Taylor, *Astrophys. J. Lett.* **195**, L51 (1975).
- [16] J. H. Taylor and J. M. Weisberg, *Astrophys. J.* **253**, 908 (1982).
- [17] B. P. Abbott et al. (LIGO Scientific, Virgo), *Phys. Rev. Lett.* **116**, 061102 (2016), 1602.03837.
- [18] B. P. Abbott et al. (LIGO Scientific, Virgo), *Phys. Rev. Lett.* **119**, 161101 (2017), 1710.05832.
- [19] P. Bagchi, A. Das, B. Layek, and A. M. Srivastava, *Phys. Lett. B* **747**, 120 (2015), 1506.03287.
- [20] A. M. Srivastava, P. Bagchi, A. Das, and B. Layek, *Pramana* **89**, 68 (2017).
- [21] P. Bagchi, B. Layek, A. Sarkar, and A. M. Srivastava, *Mon. Not. Roy. Astron. Soc.* **513**, 2794 (2022), 2111.10805.
- [22] A. Das, S. S. Dave, O. Ganguly, and A. M. Srivastava, *Phys. Lett. B* **791**, 167 (2019), 1804.00453.
- [23] M. Biswal, S. S. Dave, and A. M. Srivastava, *Phys. Lett. B* **811**, 135887 (2020), 1909.04476.
- [24] N. K. Glendenning, S. Pei, and F. Weber, *Phys. Rev. Lett.* **79**, 1603 (1997), astro-ph/9705235.
- [25] H. Heiselberg and M. Hjorth-Jensen, *Phys. Rev. Lett.* **80**, 5485 (1998), astro-ph/9801187.
- [26] L. Meitner and O. R. Frisch, *Nature (London)* **143**, 471 (1939).
- [27] R. L. Sime, *Scientific American* **278**, 80 (1998).
- [28] P. W. Anderson and N. Itoh, *Nature* **256**, 25 (1975).
- [29] T. K. Nayak, *J. Phys. Conf. Ser.* **1602**, 012003 (2020), 2008.04643.
- [30] S. Ge, X. Liang, and A. Zhitnitsky, *Phys. Rev. D* **97**, 043008 (2018), 1711.06271.
- [31] A. Atreya, A. Sarkar, and A. M. Srivastava, *Phys. Rev. D* **90**, 045010 (2014), 1405.6492.
- [32] A. Bazavov et al. (HotQCD), *Phys. Rev. D* **96**, 074510 (2017), 1708.04897.
- [33] A. Hosaka and H. Toki, *Quarks, baryons and chiral symmetry* (2001).
- [34] W. Baade and F. Zwicky, *Proceedings of the National Academy of Sciences* **20**, 259 (1934).
- [35] A. Hewish, S. J. Bell, J. D. H. Pilkington, P. F. Scott, and R. A. Collins, *Nature* **217**, 709 (1968).
- [36] R. C. Tolman, *Phys. Rev.* **55**, 364 (1939).
- [37] J. R. Oppenheimer and G. M. Volkoff, *Phys. Rev.* **55**, 374 (1939).
- [38] N. Chamel and P. Haensel, *Living Rev. Rel.* **11**, 10 (2008), 0812.3955.
- [39] B. Link, R. I. Epstein, and J. M. Lattimer, *Phys. Rev. Lett.* **83**, 3362 (1999), astro-ph/9909146.
- [40] R. N. Manchester, *J. Phys. Conf. Ser.* **932**, 012002 (2017), 1801.04318.
- [41] J. M. Weisberg, J. H. Taylor, and L. A. Fowler, *Sci. Am.* **245**, 66 (1981).
- [42] J. H. Taylor and J. M. Weisberg, *Astrophys. J.* **345**, 434 (1989).
- [43] J. M. Weisberg, D. J. Nice, and J. H. Taylor, *Astrophys. J.* **722**, 1030 (2010), 1011.0718.
- [44] L. Bildsten, *Astrophys. J. Lett.* **501**, L89 (1998), astro-ph/9804325.
- [45] D. I. Jones, *Class. Quant. Grav.* **19**, 1255 (2002), gr-qc/0111007.
- [46] B. Layek and P. Yadav, *J. Astrophys. Astron.* **41**, 14 (2020), 1904.04570.

- [47] J. Abadie et al. (LIGO Scientific), Phys. Rev. D **83**, 042001 (2011), 1011.1357.
- [48] R. N. Manchester, Class. Quant. Grav. **30**, 224010 (2013), 1309.7392.
- [49] V. Radhakrishnan and R. N. Manchester, Nature (London) **222**, 228 (1969).
- [50] C. M. Espinoza, A. G. Lyne, B. W. Stappers, and M. Kramer, Monthly Notices of the Royal Astronomical Society **414**, 1679 (2011), URL <https://doi.org/10.1111%2Fj.1365-2966.2011.18503.x>.
- [51] M. Ruderman, Nature (London) **223**, 597 (1969).
- [52] G. Baym and D. Pines, Annals of Physics **66**, 816 (1971).
- [53] A. Migdal, Nuclear Physics **13**, 655 (1959), ISSN 0029-5582, URL <https://www.sciencedirect.com/science/article/pii/0029558259902640>.
- [54] B. Haskell and A. Melatos, Int. J. Mod. Phys. D **24**, 1530008 (2015), 1502.07062.
- [55] B. Layek and P. Yadav, Mon. Not. Roy. Astron. Soc. **499**, 455 (2020), 2009.08085.
- [56] B. Layek, D. G. Venkata, and P. Yadav, Phys. Rev. D **107**, 023004 (2023), 2207.07834.
- [57] G. Baym, C. Pethick, and D. Pines, Nature (London) **224**, 673 (1969).
- [58] R. F. Archibald, V. M. Kaspi, C. Y. Ng, K. N. Gourgouliatos, D. Tsang, P. Scholz, A. P. Beardmore, N. Gehrels, and J. A. Kennea, Nature **497**, 591 (2013), 1305.6894.
- [59] S. Campana and et al., Monthly Notices of the Royal Astronomical Society **421**, 1697 (2012), URL <https://doi.org/10.1111%2Fj.1365-2966.2012.20428.x>.
- [60] P. S. Ray et al., Astrophys. J. **879**, 130 (2019), 1811.09218.
- [61] R. F. Sawyer, Phys. Rev. Lett. **29**, 382 (1972).
- [62] D. J. Scalapino, Phys. Rev. Lett. **29**, 386 (1972).
- [63] T. Tatsumi, Prog. Theor. Phys. **69**, 1137 (1983).
- [64] G.-Q. Li, C. H. Lee, and G. E. Brown, Nucl. Phys. A **625**, 372 (1997), nucl-th/9706057.
- [65] D. B. Kaplan and A. E. Nelson, Nucl. Phys. A **479**, 273c (1988).
- [66] N. K. Glendenning, Astrophys. J. **293**, 470 (1985).
- [67] A. Ohnishi, D. Jido, T. Sekihara, and K. Tsubakihara, Phys. Rev. C **80**, 038202 (2009), 0810.3531.
- [68] G. Baym, T. Hatsuda, T. Kojo, P. D. Powell, Y. Song, and T. Takatsuka, Rept. Prog. Phys. **81**, 056902 (2018), 1707.04966.
- [69] F. Özel and P. Freire, Ann. Rev. Astron. Astrophys. **54**, 401 (2016), 1603.02698.
- [70] J. Madsen, Phys. Rev. Lett. **85**, 10 (2000), astro-ph/9912418.
- [71] T. Kuroda, T. Fischer, T. Takiwaki, and K. Kotake, Astrophys. J. **924**, 38 (2022), 2109.01508.
- [72] R. F. Stark and T. Piran, Phys. Rev. Lett. **55**, 891 (1985), [Erratum: Phys.Rev.Lett. 56, 97 (1986)].
- [73] B. Giacomazzo and R. Perna, Astrophys. J. Lett. **758**, L8 (2012), 1209.0783.
- [74] B. Giacomazzo, L. Rezzolla, and N. Stergioulas, Phys. Rev. D **84**, 024022 (2011), 1105.0122.
- [75] R. W. Richardson, Phys. Rev. D **5**, 1883 (1972).
- [76] T. W. B. Kibble, J. Phys. A **9**, 1387 (1976).
- [77] T. W. B. Kibble, Phys. Rept. **67**, 183 (1980).
- [78] U. S. Gupta, R. K. Mohapatra, A. M. Srivastava, and V. K. Tiwari, Phys. Rev. D **82**, 074020 (2010), 1007.5001.
- [79] T. Vachaspati and A. Vilenkin, Phys. Rev. D **30**, 2036 (1984).
- [80] L. D. McLerran and B. Svetitsky, Phys. Rev. D **24**, 450 (1981), URL <https://link.aps.org/doi/10.1103/PhysRevD.24.450>.
- [81] B. Svetitsky, Phys. Rept. **132**, 1 (1986).
- [82] T. Bhattacharya, A. Gocksch, C. Korthals Altes, and R. D. Pisarski, Nucl. Phys. B **383**, 497 (1992), hep-ph/9205231.
- [83] B. Layek, A. P. Mishra, and A. M. Srivastava, Phys. Rev. D **71**, 074015 (2005), hep-ph/0502250.
- [84] U. S. Gupta, R. K. Mohapatra, A. M. Srivastava, and V. K. Tiwari, Phys. Rev. D **86**, 125016 (2012), 1111.5402.
- [85] R. K. Mohapatra and A. M. Srivastava, Phys. Rev. C **88**, 044901 (2013), 1210.4718.
- [86] M. G. Alford, K. Rajagopal, and F. Wilczek, Phys. Lett. B **422**, 247 (1998), hep-ph/9711395.
- [87] C. J. Horowitz and K. Kadau, Phys. Rev. Lett. **102**, 191102 (2009), 0904.1986.
- [88] D. A. Baiko and A. I. Chugunov, Mon. Not. Roy. Astron. Soc. **480**, 5511 (2018), 1808.06415.
- [89] K. Makishima, T. Enoto, J. S. Hiraga, T. Nakano, K. Nakazawa, S. Sakurai, M. Sasano, and H. Murakami, Phys. Rev. Lett. **112**, 171102 (2014), 1404.3705.
- [90] R. Abbott et al. (LIGO Scientific, Virgo), Astrophys. J. Lett. **902**, L21 (2020), 2007.14251.
- [91] J. Aasi et al. (LIGO Scientific), Astrophys. J. **785**, 119 (2014), 1309.4027.
- [92] D. Kleppner and R. Kolenkow, *An Introduction to Mechanics* (Cambridge University Press, 2014), ISBN 9780521198110, URL <https://books.google.co.in/books?id=Se7CAQAAQBAJ>.
- [93] H. Goldstein, *Classical Mechanics* (Pearson Education, 2002), ISBN 9788177582833, URL <https://books.google.co.in/books?id=Spy6xHWFJIEC>.
- [94] S. A. Colgate and A. G. Petschek, Astrophys. J. **248**, 771 (1981).
- [95] P. Bagchi, B. Layek, A. Sarkar, and A. M. Srivastava, *Manuscript in preparation* (2023).
- [96] K. S. Thorne and A. Campolattaro, Astrophysical Journal p. 591 (1967).
- [97] R. Price and K. S. Thorne, Astrophys. J. **155**, 163 (1969).
- [98] K. S. Thorne, Astrophys. J. **158**, 1 (1969).
- [99] K. S. Thorne, Astrophys. J. **158**, 997 (1969).
- [100] M. Zimmermann and E. Szedenis, Phys. Rev. D **20**, 351 (1979), URL <https://link.aps.org/doi/10.1103/PhysRevD.20.351>.
- [101] P. D. Lasky, Publ. Astron. Soc. Austral. **32**, e034 (2015), 1508.06643.
- [102] L. Keer and D. I. Jones, Mon. Not. Roy. Astron. Soc. **446**, 865 (2015), 1408.1249.
- [103] K. Riles, Prog. Part. Nucl. Phys. **68**, 1 (2013), 1209.0667.
- [104] J. Weber, Phys. Rev. Lett. **18**, 498 (1967).
- [105] J. Weber, Phys. Rev. Lett. **22**, 1320 (1969).
- [106] O. D. Aguiar, Res. Astron. Astrophys. **11**, 1 (2011), 1009.1138.
- [107] S. Husa, Gen. Rel. Grav. **41**, 1667 (2009).
- [108] G. Hobbs and S. Dai, Natl. Sci. Rev. **4**, 707 (2017), 1707.01615.
- [109] F. J. Dyson, Astrophys. J. **156**, 529 (1969).

- [110] I. Lopes and J. Silk, *Astrophys. J.* **844**, 39 (2017), 1707.06249.
- [111] I. Lopes and J. Silk, *Astrophys. J.* **807**, 135 (2015), 1507.03212.
- [112] I. Lopes and J. Silk, *Astrophys. J.* **794**, 32 (2014), 1405.0292.
- [113] T. Hinderer, *Astrophys. J.* **677**, 1216 (2008), 0711.2420.
- [114] S. M. Carroll, *Spacetime and Geometry* (Cambridge University Press, 2019), ISBN 978-0-8053-8732-2, 978-1-108-48839-6, 978-1-108-77555-7.
- [115] C. J. Krüger, W. C. G. Ho, and N. Andersson, *Phys. Rev. D* **92**, 063009 (2015), 1402.5656.
- [116] D. Lai, *Mon. Not. Roy. Astron. Soc.* **270**, 611 (1994), astro-ph/9404062.
- [117] L. Ju, D. Blair, and C. Zhao, *Reports on Progress in Physics* **63**, 1317 (2000), ISSN 0034-4885.